SYNTHESIS AND CHARACTERISATION OF BI-METALLIC PROMOTED VANADYL PYROPHOSPHATE CATALYSTS USING ULTRASONIC METHOD

ADAM LEONG WENG KAI

A project report submitted in partial fulfilment of the requirements for the award of Bachelor of Engineering (Hons.) Chemical Engineering

Lee Kong Chian Faculty of Engineering and Science
Universiti Tunku Abdul Rahman

September 2017

DECLARATION

I hereby declare that this project report is based on my original work except for citations and quotations which have been duly acknowledged. I also declare that it has not been previously and concurrently submitted for any other degree or award at UTAR or other institutions.

Signature : _____

Name : Adam Leong Weng Kai

ID No. : 13UEB00728

Date : 25/8/2017

APPROVAL FOR SUBMISSION

I certify that this project report entitled **"SYNTHESIS AND CHARACTERISATION OF BI-METALLIC PROMOTED VANADYL PYROPHOSPHATE CATALYSTS USING ULTRASONIC METHOD"** was prepared by **ADAM LEONG WENG KAI** has met the required standard for submission in partial fulfilment of the requirements for the award of Bachelor of Engineering (Hons.) Chemical Engineering at Universiti Tunku Abdul Rahman.

Approved by,

Signature : _____

Supervisor : DR. LEONG LOONG KONG

Date : _____

ACKNOWLEDGEMENTS

I would like to thank everyone who had contributed to the successful completion of this project. I would like to express my gratitude to my research supervisor, Dr. Leong Loong Kong for his time and patience in guiding me and providing me invaluable advice.

Moreover, I would like to thank my parents for their constant support and my fellow course mates for being helpful and thoughtful during the entire project. I would also like to extend my gratitude to Mr. Chin Kah Chun and Ms. Kang Jo Yee for their guidance in carrying out the research. Without their guidance, this research would not come to completion.

ABSTRACT

Precursors to produce vanadyl pyrophosphate (VPO) catalyst were prepared via sesquihydrate route using 1-butanol as reducing agent. Sonochemical technique is used to synthesise the precursor. Precursor is calcined at 460 °C to produce vanadyl pyrophosphate catalyst. The catalyst showed amorphous structure in X-ray Diffraction Analysis (XRD) and Fourier-Transform Infrared (FTIR) is used instead to identify the identity of the catalyst. The presence of P – O and V = O proved that the catalyst obtained is attributed to vanadyl pyrophosphate phase. Scanning Electron Microscopy (SEM) shows blocky structure for undoped VPO catalyst and rod-like structure for cobalt doped catalyst. Cobalt has more prominent promotional effect than copper in VPO catalyst as the micrograph bi-metallic doped VPO catalyst features the distinctive rod-like structure similar to cobalt doped VPO catalyst. P/V atomic ratio determined from Energy Dispersive X-ray (EDX) and Inductively Coupled Plasma – Optical Emission Spectroscopy (ICP-OES) are in the range of optimal values in producing vanadyl pyrophosphate catalysts. Cobalt is also more dominant as can be observed from P/V atomic ratio, the bi-metallic doped VPO catalyst has a P/V atomic ratio that is closer to cobalt doped VPO catalyst. In redox titration, it can be observed that cobalt enhances the promotional effect of copper in bi-metallic VPO catalyst where more V^{5+} phases are formed. Temperature Programming Reduction (TPR) analysis shows a lower reduction activation energy for bi-metallic doped VPO catalyst and this may be the synergistic effect between cobalt and copper dopant in VPO catalyst.

TABLE OF CONTENTS

DECLARATION **ii**
APPROVAL FOR SUBMISSION **iii**
ACKNOWLEDGEMENTS **v**
ABSTRACT **vi**
TABLE OF CONTENTS **vii**
LIST OF TABLES **x**
LIST OF FIGURES **xi**
LIST OF SYMBOLS / ABBREVIATIONS **xiii**
LIST OF APPENDICES **xiv**

CHAPTER

1 INTRODUCTION **1**
1.1 Definitions of Catalysis 1
1.2 Catalysed Reactions and Non-Catalysed Reactions 1
1.3 Types of Catalyst 2
1.3.1 Homogeneous Catalyst 2
1.3.2 Heterogeneous Catalyst 3
1.3.3 Biocatalyst 4
1.3.4 Desirable Properties of Catalyst 4
1.3.5 Importance of Catalyst 5
1.4 Problem Statement 5
1.5 Aims and Objectives 6

2 LITERATURE REVIEW **7**
2.1 Production of Maleic Anhydride from *n*-Butane 7
2.2 Vanadyl Pyrophosphate Catalyst 8
2.2.1 Structure of Vanadyl Pyrophosphate Catalyst 8

2.2.2 Mechanism of Vanadyl Pyrophosphate Catalyst on Oxidation of *n*-Butane to Maleic Anhydride 10
2.3 Vanadyl Pyrophosphate Catalyst Preparation Route 11
2.3.1 Hemihydrate (Aqueous Route) 11
2.3.2 Hemihydrate (Organic Route) 12
2.3.3 Hemihydrate (Dihydrate Route) 12
2.3.4 Sesquihydrate Route 13
2.4 Sonochemical Synthesis 13
2.5 Parameters of Vanadyl Pyrophosphate Catalyst 14
2.5.1 Calcination Duration 14
2.5.2 Calcination Temperature 15
2.5.3 Calcination Environment 15
2.5.4 Doped System 16
2.5.5 P/V Atomic Ratio 16

3 METHODOLOGY 18
3.1 Materials 18
3.2 Methodology 18
3.3 Preparation of Vanadyl Phosphate Dihydrate Precursor 19
3.4 Preparation of Vanadyl Hydrogen Phosphate Sesquihydrate Precursor 19
3.5 Calcination 19
3.6 Characterisation of Catalyst 20
3.6.1 X-ray Diffraction Analysis (XRD) 20
3.6.2 Redox Titration 22
3.6.3 Scanning Electron Microscope (SEM) 23
3.6.4 Energy Dispersive X-ray (EDX) 24
3.6.5 Temperature Programmed Reduction (TPR) 25
3.6.6 Inductively Coupled Plasma – Optical Emission Spectroscopy (ICP-OES) 27
3.6.7 Fourier-Transform Infrared (FTIR) 28

4 RESULTS AND DISCUSSION 30

	4.1	Introduction	30
	4.2	X-Ray Diffraction (XRD) Analysis	30
	4.3	Fourier-Transform Infrared Spectroscopy (FTIR)	31
	4.4	Scanning Electron Microscope (SEM)	33
	4.5	Energy Dispersive X-ray Spectrometry (EDX)	34
	4.6	Inductively Coupled Plasma - Optical Emission Spectroscopy (ICP-OES)	35
	4.7	Redox Titration	36
	4.8	Temperature-Programmed Reduction (TPR)	37
5	**CONCLUSION AND RECOMMENDATIONS**		**41**
	5.1	Conclusion	41
	5.2	Recommendations	42
REFERENCES			**43**
APPENDICES			**47**

LIST OF TABLES

Table 2.1: Comparisons between Fixed bed Reactor and Fluidised Bed Reactor 8

Table 4.1: Compositions of VPO Samples and the Average P/V Atomic Ratio 34

Table 4.2: P/V Atomic Ratio from ICP-OES 35

Table 4.3: Average Oxidation Number of Vanadium from Redox Titration 37

Table 4.4: Total amount of O_2 removed from the VPOs catalysts. 38

LIST OF FIGURES

Figure 1.1: Energy Profile for Catalysed and Non-catalysed Process 2

Figure 1.2: Lock and Key Scheme. 4

Figure 2.1: VO_6 and PO_4 Crystal Structures (blue is vanadium, red is oxygen, yellow is phosphate) 9

Figure 2.2: Single Ideal VPO Strand 9

Figure 2.3: Proposed Reaction Mechanism on Oxidation of *n*-butane to Maleic Anhydride. 10

Figure 3.1: Set-up of Ultrasound Equipment 19

Figure 3.2: Schematics of the X-ray Diffraction. 20

Figure 3.3: Flowchart on the Working Principle of XRD 21

Figure 3.4: Shidmadzu 6000 XRD 22

Figure 3.5: Hitachi S-3400 24

Figure 3.6: Different Radiation Emission During Excitation of Electrons 25

Figure 3.7: Thermo Electron TPDRO 1100 26

Figure 3.8: A typical ICP-OES Diagram 27

Figure 3.9: Perkin Elmer Optical Emission Spectrometer Optima 7000 DV 28

Figure 3.10: Nicolet iS 10 FTIR Spectrometer 29

Figure 4.1: XRD Patterns of Undoped and Doped VPO Samples 31

Figure 4.2: FTIR Spectra of VPO Samples Undoped and Doped 32

Figure 4.3: SEM Micrographs of (a) VPOBulk (b) VPOCo1% (c) VPOCu1% (d) VPOCu1%Co1% at ×10000 magnification 33

Figure 4.4: TPR Profiles of VPOs Catalysts 39

Figure 4.5: Comparison of amount of oxygen removed from catalyst between V^{4+} and V^{5+} phases 40

LIST OF SYMBOLS / ABBREVIATIONS

o-H_3PO_4	*Ortho*-phosphoric acid
NH_2OH	Hydroxylamine
V_2O_5	Vanadium pentoxide
VPO	Vanadium phosphorous oxide, vanadyl pyrophosphate
$VOHPO_4 \cdot 0.5H_2O$	Vanadyl Hydrogen Phosphate Hemihydrate
$VOHPO_4 \cdot 1.5H_2O$	Vanadyl Hydrogen Phosphate Sesquihydrate
$VOPO_4 \cdot 2H_2O$	Vanadyl Phosphate Dihydrate
V^{3+}	Vanadium at oxidation state of +3
V^{4+}	Vanadium at oxidation state of +4
V^{5+}	Vanadium at oxidation state of +5
V^{3+}	Concentration of V^{3+}
V^{4+}	Concentration of V^{4+}
V^{5+}	Concentration of V^{5+}
V_{AV}	Average oxidation number of vanadium
BET	Brunauer-Emmett-Teller Analysis
EDX	Energy Dispersive X-ray Spectrometry
SEM	Scanning Electron Microscope
TPR	Temperature-Programmed Reduction
XRD	X-ray Diffraction Analysis
L	Average crystallite size
K	Shape factor of crystallite. About 0.89 for spherical crystals
λ	Wavelength of x-ray
β	Full Width at Half Maximum
θ	Diffraction angle
T_m	Temperature maxima
E_R	Reduction activation energy

LIST OF APPENDICES

APPENDIX A: Reactant and Dopants Calculations 47

APPENDIX B: Preparation of Solutions Used in Redox Titration 49

APPENDIX C: Redox Titration Procedure 52

APPENDIX D: Preparation of Solutions Used for ICP-OES 54

APPENDIX E: Procedure for ICP-OES Analysis 60

APPENDIX F: P/V Atomic Ratio from ICP-OES analysis 63

APPENDIX G: Calculation for Average Oxidation State of Vanadium (V_{AV}) 64

APPENDIX H: Calculation for Reduction Activation Energy (E_r) for TPR Analysis 67

APPENDIX I: Calculation for Amount of Oxygen Removed 68

CHAPTER 1

INTRODUCTION

1.1 Definitions of Catalysis

The history of catalysis dates back to about 200 years ago where the process is observed on the conversion of starch to glucose catalysed by concentrated acid and combining hydrogen and oxygen using platinum catalyst. The term "catalysis" is derived from Greek words "*kata*" which means down and "*lyein*" which means loosen. Swedish chemist, Jons Berzelius believed that catalysis increases the rate of reaction of a chemical reaction without actually participating in the reaction. This assumes the catalyst is not consumed during the chemical reaction. This statement is false as quite often catalyst is consumed during the reaction but regenerated back to its original state (Mazur, 2001). From the Gold Book, catalysis refers to a process where the rate of reaction is increased by a substance without changing the overall standard Gibbs energy change in the reaction (IUPAC, 2014).

1.2 Catalysed Reactions and Non-Catalysed Reactions

Chemical reaction is a process of bond-breaking and bond-forming of reactants and products. During bond-breaking process, energy is absorbed to break stable bonds while during bond-forming process, energy is released to form new bonds. In an exothermic reaction, the energy of the products is lower than the energy of reactants as energy is released during the process. However, in an endothermic reaction, as energy is absorbed, the energy of the products is higher than reactants (Farrauto et al., 2016).

In a catalysed reaction, catalyst is used to provide an alternative reaction pathway that requires lower activation energy compared to non-catalysed reaction. It can be seen from Figure 1.1 that catalysed reaction only requires energy, E_{Mn} for the reaction to occur whereas non-catalysed reaction require high activation energy, E_{NC} for the reaction to take place (Farrauto et al., 2016).

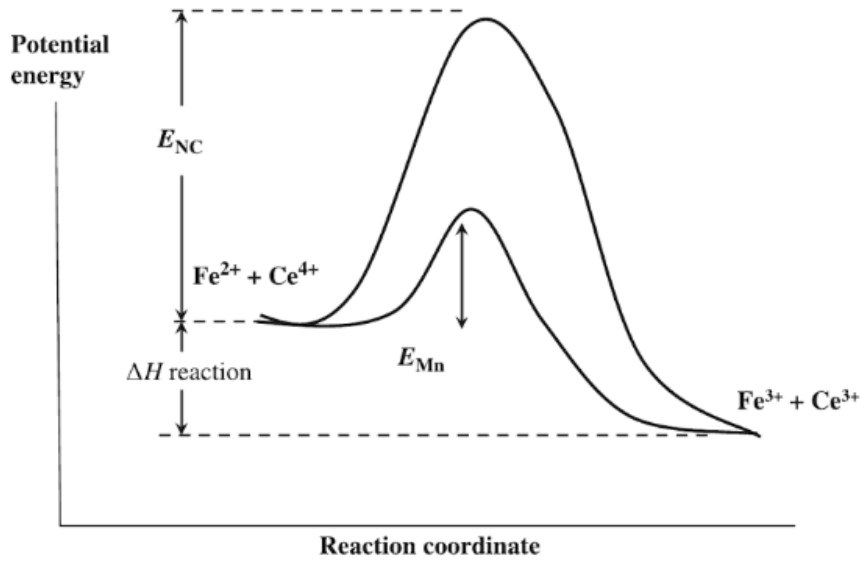

Figure 1.1: Energy Profile for Catalysed and Non-catalysed Process

What differs catalyst from reactants is that catalyst will return to its original state after the reaction. Although catalyst participates in the chemical reaction, catalyst only merely interact with the reactants to form intermediate species that will proceed to form the desired product. Catalyst other hand, returns to its original state (Farrauto et al., 2016).

1.3 Types of Catalyst

Catalyst comes in a variety of forms and compositions. As catalyst is highly specific to a particular process, many different types of catalyst has been discovered and employed. Generally, all catalyst falls into one of the three categories: homogeneous, heterogeneous and biocatalyst.

1.3.1 Homogeneous Catalyst

Catalysts that has the same phase as reactants are known as homogeneous catalyst. Homogeneous catalysts have many advantages including high selectivity and high controllability. This is because when the catalyst is same phase as the reactants, reactants can easily access all the active site even without a mixing system installed. Moreover, it is also possible to modify and fine-tune the performance of homogeneous catalyst to increase its selectivity (Chorendorff and Niemantsverdriet, 2003).

However, homogenous catalyst is not common used in the industries due to difficulties in separating the catalyst from the product. Many separation units available

in the market is based on the volatility of the product and in other words, temperature. Homogeneous catalysts are often sensitive to temperature and will usually decompose below 150 °C. This limits the application of homogeneous catalyst in the industry (Chorendorff and Niemantsverdriet, 2003).

Homogenous catalyst is usually used in production of pharmaceutical components where a catalyst known as ligand is used to increase the selectivity of organometallic complexes (Chorendorff and Niemantsverdriet, 2003). Other commercialised applications of homogeneous catalyst typically involve volatile products that can be separated at low cost (Cole-Hamilton, 2003).

1.3.2 Heterogeneous Catalyst

Unlike homogeneous catalyst which exist same phase as the reactants, heterogeneous catalyst exists as solid substances. In general, heterogeneous catalyst can be classified into two categories: unsupported or supported. In a supported heterogeneous catalyst, active component from the catalyst is well dispersed into a porous and inert support whereas unsupported heterogeneous catalyst is not dispersed into a support. The purpose of this support mainly is to increase the effective surface area and maintain the dispersion of active phase. As effective surface area is related to the number of catalytic sites available, increase in effective surface area would increase the number of catalytic sites as well as the rate of reaction. Support can also increase the durability of catalyst by reducing the collision among the catalyst. Common materials used as support are Al_2O_3, zeolites and SiO_2 (Farrauto et al., 2016).

Besides supports, selection of active species and promoter also has an effect on the performance of the catalyst. It is found that Group 8B elements such as iron, cobalt and nickel and vanadium from Group 5B show great catalytic properties in their metals or oxides form. However, it is important to know catalyst used in petrochemical industry often synthesise their catalyst with specific combinations or formulae to increase their selectivity on the desired reaction. The active species in a catalyst usually not present in its elementary state, but may be present as an oxide (Farrauto et al., 2016).

Promoters are added into the catalyst to facilitate the catalytic reaction by the active species. Promoters can be further divided into structural and electronic promoters based on their method of promotion. Structural promoter stabilises the active species dispersion and as well as introducing intercalation in the catalyst to

enhance surface area. Electronic promoters on the other hand, improve the surface reaction (Farrauto et al., 2016).

1.3.3 Biocatalyst

Biocatalyst or more commonly known as enzymes are catalyst that are naturally produced by living organism. Biocatalyst are normally highly selective due to the structure which consists of large molecule of protein that has an active site which will only bind with specific shape of substrate. The process where the substrates are bounded by the active site according to their shape is known as a "Lock and Key" scheme as shown in Figure 1.2. However, biocatalyst is very sensitive to heat and only able to function within a certain narrow temperature range (Chorendorff and Niemantsverdriet, 2003).

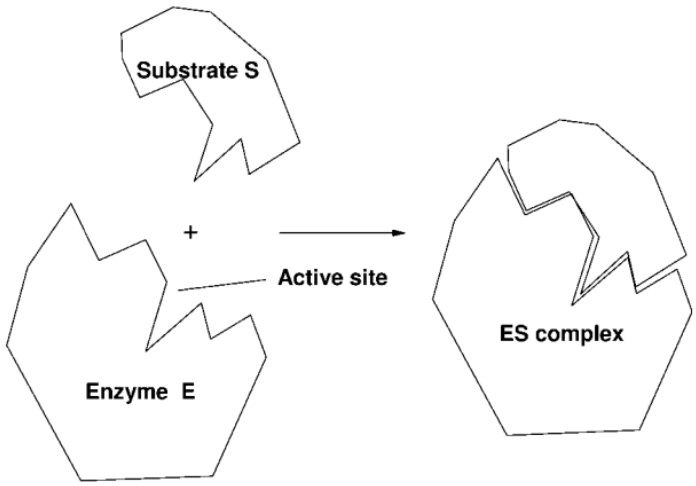

Figure 1.2: Lock and Key Scheme.

The advantages of biocatalysts compared to homogeneous and heterogeneous catalysts is biocatalysts do not disturb the thermodynamics of the reaction. In addition, biocatalysts are highly selective, increasing production of desired product (Johannes et al., 2006).

1.3.4 Desirable Properties of Catalyst

Although a catalyst can increase the rate of reaction, a high rate of reaction does not always mean it has a yield of desired product. It is dependent on the selectivity of the catalysts as well. A high selectivity catalyst means that the main reaction is favoured

over the side reaction and thus increasing the yield of the desired product. Catalytic activity should be at maximum at reaction condition. Besides that, durability and possibility to regenerate are also important to consider (Bartholomew and Farrauto, 2005).

Durability properties is especially important when the reactor used is a fluidised bed reactor. This is because in fluidised bed reactor, the rate of collision is very high and catalyst may be eroded after multiple times of collision. As a result, the operating cost of the plant increases as maintenance or replacement of catalyst has to be done frequently. To rectify this issue, normally the catalyst is supported to reduce the number of collision (Yang, 2003).

Catalyst regeneration is unavoidable in many reactions as catalyst can be deactivated due to many reasons. Regeneration of catalyst can reduce the operating cost of the plant as catalyst can be regenerated multiple times (Bartholomew and Farrauto, 2005).

1.3.5 Importance of Catalyst

Chemical reactions in general depends on temperature, pressure, concentration of reactant as well as the contact time in the reactor. At higher temperature and pressure, the reactions not only will take place at higher rate but also increase in production. However, to achieve reasonable rate of reaction, severe operating conditions may require and this can contribute to increase in operating cost as well as high difficulty to control. Besides that, temperature of the reactor cannot be as high as possible due to thermodynamic limitations to conditions under which the products are formed. For example, to produce ammonia without catalyst, very high temperature is required to break the triple bond of nitrogen molecule but if temperature exceeds 600 °C, ammonia will not be produced anymore (Chorendorff and Niemantsverdriet, 2003).

The use of catalyst can reduce the severe operating conditions significantly. Without catalyst, chemical industry would still be relying on non-catalysed reactions. Catalyst enables the reaction to take place with a suitable thermodynamic regime, making the process more economical (Chorendorff and Niemantsverdriet, 2003).

1.4 Problem Statement

Maleic anhydride is a commodity product that is used to produce unsaturated polyesters and butanediol. The reaction of oxidation of *n*-butane to maleic anhydride

area amongst the most studied in catalysis. As pointed by Ballarini et al. (2006), latest patent review reported that the highest selectivity and conversion to maleic anhydride from *n*-butane is only about 65 % and 86 % respectively.

The low selectivity of the reaction is due to the presence of parallel side reactions where *n*-butane undergoes combustion and maleic anhydride produced undergoes oxidative degradation to produce acetic acid and acrylic acids. Moreover, when conversion of *n*-butane to maleic anhydride increases to about 70-80 %, the selectivity towards maleic anhydride will decrease dramatically. The highly exothermic reaction also causes catalyst deactivation issue as sintering of catalyst occurs (Ballarini et al., 2006).

It was found that doping of vanadyl pyrophosphate (VPO) catalyst can actually improve the performance of the catalyst in oxidation of *n*-butane. In this project, the doped catalyst will be characterised to determine its physical, chemical and reactivity properties.

1.5 Aims and Objectives

The objectives of this project were:

1. To synthesise bulk VPO catalyst, Cu-doped VPO catalysts, Co-doped VPO catalysts and Cu-Co doped VPO catalysts using sonochemical technique.
2. To study the effect of Cu and Co towards the physical properties, chemical properties and also the reactivity properties of the synthesised VPO catalyst.

CHAPTER 2

LITERATURE REVIEW

2.1 Production of Maleic Anhydride from *n*-Butane

Transition from using benzene as feedstock to *n*-butane took roughly 15 years and many earlier maleic acid production plants maintains an interchangeability of feedstock feature on their reactor to allow interchange of feedstock depending on economic conditions. The general chemical equation for the primary reaction (2.1) and secondary reaction (2.2) of oxidation of *n*-butane to maleic anhydride can be seen below (Musa, 2016):

$$C_4H_{10} + 3.5O_2 \longrightarrow C_4H_2O_3 + 4H_2O \quad (2.1)$$

$$C_4H_2O_3 + \frac{(6-m)}{2}O_2 \longrightarrow mCO + (4-m)CO_2 + H_2O \quad (2.2)$$

Two most common types of reactor used are fixed bed reactor and fluidised bed reactor. Almost all maleic anhydride process plants are equipped with reactor, gas cooler, separator, scrubber, condenser and product column collector. When operating with fixed bed reactor, hotspots in the reactor and composition of feedstock mixture are important. Severe hotspots in the reactor can reduce catalyst life, increasing maintenance cost of the plant while monitoring of feedstock composition is required to ensure the composition is below the flammability limit in air. On the other hand, fluidised bed reactor which often operate at 360 °C - 460 °C has lesser hotspot problem. This is because heat generated during the oxidation process can be removed by steam coil located inside the reactor efficiently as a result of direct contact with fluidised solid in the reactor (Musa, 2016). Table 2.1 shows comparisons between a fixed bed reactor and fluidised bed reactor has been reported by Wellauer (1985) in 1985.

As mentioned by Musa (2016), “VPO is the catalyst that change the maleic anhydride industry”. The catalyst mentioned here is VPO and this catalyst played an important role in the oxidation process of *n*-butane to maleic anhydride.

Table 2.1: Comparisons between Fixed bed Reactor and Fluidised Bed Reactor

	Fixed bed reactor	**Fluidised bed reactor**
Capital Requirement	Large	Less significant
Design knowledge	Clear	Emerging
Pressure Drop	Major	Minor
Back Mixing	Insignificant	Challenging
Heat Transfer	Not good	Good
Regeneration of catalyst during operation	Challenging	Minor

2.2 Vanadyl Pyrophosphate Catalyst

The term "VPO" has been widely used to represent vanadyl diphosphate and vanadyl pyrophosphate where both of this compound has the same chemical formula, $(VO)_2P_2O_7$. VPO is a type of vanadium oxide catalyst that contains VO_6 and PO_4 that sharing the same oxygen bond. Vanadium oxide can exist in +5, +4, +3, and +2 oxidation states but +5 and +4 oxidation states is the active element in the VPO catalyst that promote the oxidation of *n*-butane to maleic anhydride (Musa, 2016).

2.2.1 Structure of Vanadyl Pyrophosphate Catalyst

The structure of VPO catalyst originates from two basic structures: VO_6 and PO_4. The structure of VO_6 is a distorted octahedron where the central vanadium atom is coordinated to six oxygen atoms. However, as a stronger double bond is present between vanadium atom to an oxygen atom, the bond length between the vanadium atom and the oxygen atom is shorter. This creates a distortion in the octahedron as three ranges of bond length; short, normal and long are present in the octahedron as shown in Figure 2.1A. Approximate value for bond lengths of short, normal and long are 1.6 A, 2 A and 2.3 A, respectively (Musa, 2016).

PO_4, on the other hand is tetrahedron where the central phosphate atom is coordinated to four oxygen atoms as shown in Figure 2.1B. As there is no double bond or triple bond present in the crystal structure, the crystal structure of PO_4 is not distorted and all the bond lengths are equivalent, approximately 1.5 A (Musa, 2016).

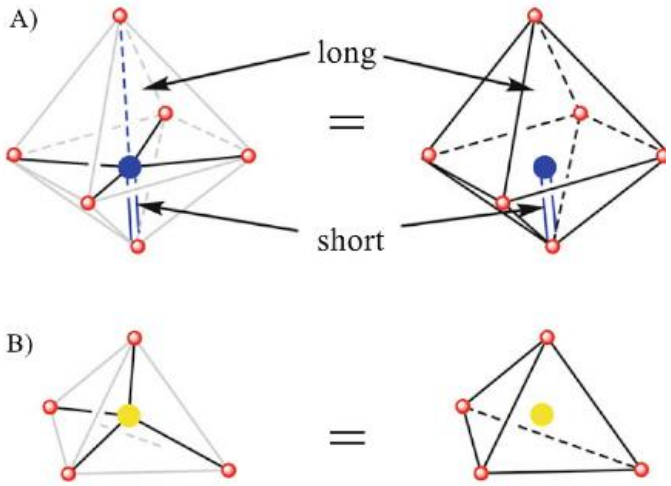

Figure 2.1: VO_6 and PO_4 Crystal Structures (blue is vanadium, red is oxygen, yellow is phosphate)

To produce VPO crystal structure, two VO_6 distorted octahedron are bonded in a trans-oriented manner, which means the two octahedron are at opposite direction. The four oxygen atoms with the normal bond length to central vanadium are connected to the PO_4 by sharing the oxygen atoms. Two types of VPO general structure prevail: one consist of single VO_6 distorted octahedron and the other consist of a pair of VO_6 distorted octahedron as shown in Figure 2.2. From this single individual strand, a more complex crystalline sheet can be obtained when multiple strand is connected together. However, presence of impurities and structural defects makes this ideal VPO strand impossible to exist in VPO catalyst in the industry (Musa, 2016).

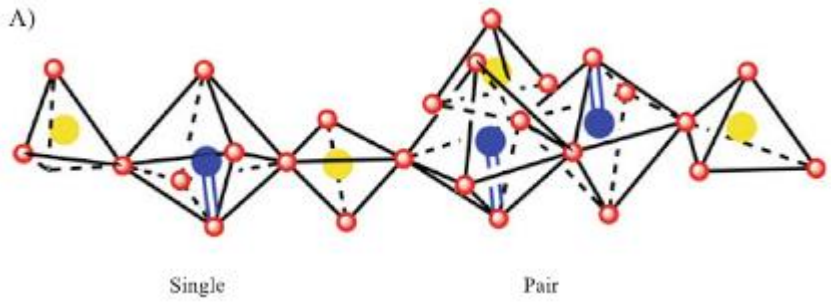

Figure 2.2: Single Ideal VPO Strand

2.2.2 Mechanism of Vanadyl Pyrophosphate Catalyst on Oxidation of *n*-Butane to Maleic Anhydride

A reaction mechanism for oxidation of *n*-butane to maleic anhydride catalysed by VPO catalyst as shown in Figure 2.3 was suggested by Busca and Centi in 1989. It was suggested that the *n*-butane reaction can have two routes to form maleic anhydride in the presence of VPO catalyst. Both routes are believed to have equal selectivity over one another. However, Route A based on Figure 2.3 have a faster rate of reaction compared to Route B. This is indicated by the enhanced reactivity in the presence of gaseous oxygen (Musa, 2016).

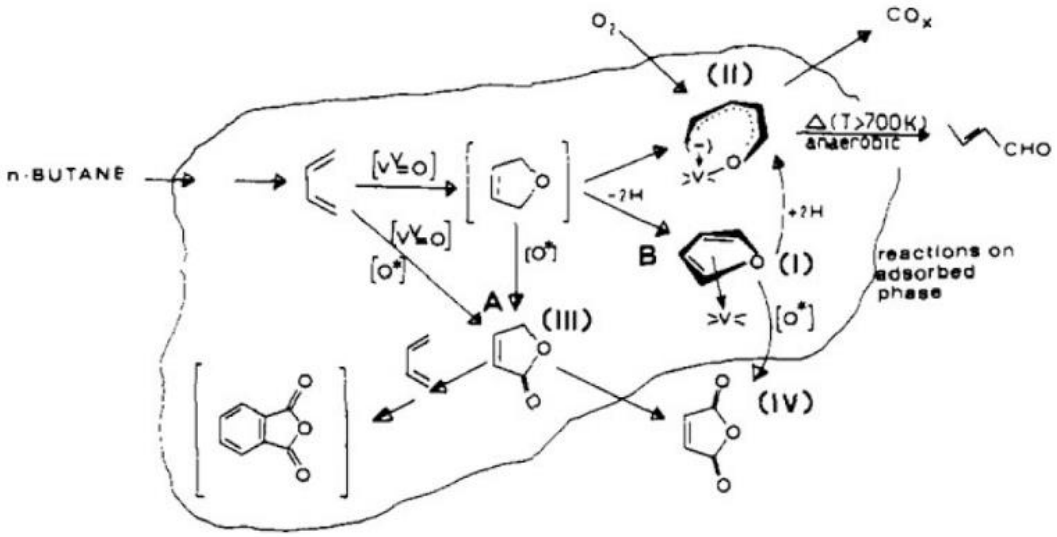

Figure 2.3: Proposed Reaction Mechanism on Oxidation of *n*-butane to Maleic Anhydride.

In Route A, *n*-butane is first reacted to form butadiene under high temperature condition. Butadiene is then converted to dihydrofuran intermediate via oxygen insertion from V^5=O. The two double bonds presence in butadiene will be broken and bond to the same oxygen atom through a process known as electrophilic addition. The intermediate can then reacted with oxygen labile species, (O*) to form γ-crotonolactone. However, it is not necessarily to form dihydrofuran intermediate as butadiene can also directly forms γ-crotonolactone by bonding with (O*) and insertion of oxygen from V^5=O at the same time. Further oxidation of γ-crotonolactone will yield maleic anhydride. However, γ-crotonolactone can react with butadiene to from

phthalic anhydride if the contact time of the intermediate with butadiene is too long (Musa, 2016).

The second route, Route B begins similar to Route A where *n*-butane forms butadiene and forms dihydrofuran subsequently. In Route B, dihydrofuran undergoes a dehydrogenation process to form furan(I) intermediate which can then be reacted with (O*) to produce maleic anhydride. Nevertheless, furan(I) intermediate can also form crotonaldehyde and carbon oxides. This is due to strong Lewis acid site interactions at the VPO surface, which causes furan(I) intermediate to acts as hydrogen transfer agent and promotes other hydrocarbon species present in the reaction (Musa, 2016).

Although there have been many other proposed reaction mechanisms of VPO on oxidation *n*-butane to maleic anhydride, researchers have yet to find a definite answer. Even now, researchers are still striving to improve VPO catalyst performance by investigating different catalyst preparation techniques and composition to have better understanding on the mechanism.

2.3 Vanadyl Pyrophosphate Catalyst Preparation Route

VPO catalyst can be synthesised by calcination of two types precursors: vanadyl hydrogen phosphate hemihydrate, $VOHPO_4 \cdot 0.5H_2O$ and vanadyl hydrogen phosphate sesquihydrate, $VOHPO_4 \cdot 1.5H_2O$. Preparation of hydrogen phosphate hemihydrate can be further divided into three routes: organic, dihydrate and aqueous route.

2.3.1 Hemihydrate (Aqueous Route)

The first method used to produce VPO catalyst precursor is via the aqueous route. Hydrochloric acid is used in this route to act as reducing agent by reducing V^{5+} from vanadium pentoxide to V^{4+}. Several alternative reducing agents had been proposed such as oxalic acid, lactic acid, phosphoric acid and NH_2OH (Jackson and Hargreaves, 2009).

Vanadium pentoxide is first refluxed with hydrochloric acid before adding phosphoric acid to allow reaction in Equation 2.3 to take place. It was found that the VPO catalysts prepared using aqueous route have a cubic morphology and a low surface area (Jackson and Hargreaves, 2009).

$$V_2O_5 + H_3PO_4 + HCl \longrightarrow VOHPO_4 \cdot 0.5H_2O \quad (2.3)$$

2.3.2 Hemihydrate (Organic Route)

In organic route, V^{5+} present in vanadium pentoxide is reduced to by V^{4+} by with alcohol such as isobutanol and benzyl alcohol. The alcohol servers as both the reducing agent and organic solvent. After vanadium pentoxide is added with the alcohol, the mixture is refluxed for an hour, followed by a reaction with phosphoric acid and finally yielding $VOHPO_4 \cdot 0.5H_2O$ as shown in Equation 2.4 (Jackson and Hargreaves, 2009).

$$V_2O_5 + H_3PO_4 + alcohol \longrightarrow VOHPO_4 \cdot 0.5H_2O \quad (2.4)$$

VPO catalysts synthesised via organic route were found to have platelet crystalline morphology and the size of the platelets are depended on the type of organic solvent used. For example, using isobutanol as the alcohol will cause platelets to lump together, forming a rosette morphology while using sec-butyl alcohol allows platelets to form. Moreover, crystal structure of $VOHPO_4 \cdot 0.5H_2O$ is also dependant on the type of solvent. Using alcohol with large molecule such as benzyl alcohol can induce stacking faults in the platelets which in turn, improves catalyst performance due to increase in surface area (Benziger et al., 1997).

2.3.3 Hemihydrate (Dihydrate Route)

Dihydrate route is two step procedure which involves reduction of a dihydrate, $VOPO_4 \cdot 2H_2O$ by alcohol to form hemihydrate, $VOHPO_4 \cdot 0.5H_2O$. Water is used as the solvent in this route instead of alcohol as compared to organic route. Vanadium pentoxide is first reacted with phosphoric acid to form $VOPO_4 \cdot 2H_2O$ in the presence of water. $VOPO_4 \cdot 2H_2O$ is then recovered and dried before proceeding to the second step. In the second step, $VOPO_4 \cdot 2H_2O$ is refluxed with alcohol to form $VOHPO_4 \cdot 0.5H_2O$ (Jackson and Hargreaves, 2009).

Similar to organic route, the crystal structure and morphology is determined by the type of alcohol used. Dihydrate reflux with primary alcohol has higher tendency to form rosette structure in the VPO catalyst which have high surface area whereas secondary alcohol tends to form thick platelet which have lower surface area. The reaction is shown in Equation 2.5 (Védrine et al., 2013).

$$V_2O_5 + H_3PO_4 + H_2O \longrightarrow VOPO_4 \cdot 2H_2O \xrightarrow{\text{alcohol}} VOHPO_4 \cdot 0.5H_2O \qquad (2.5)$$

2.3.4 Sesquihydrate Route

A more recent studies found that VPO catalyst can also be produced via a sesquihydrate precursor $VOHPO_4 \cdot 1.5H_2O$. The sesquihydrate precursor can be produced by reducing vanadyl hydrogen phosphate dihydrate $VOPO_4 \cdot 2H_2O$ by refluxing in less-reductive alcohols such as 1-butanol. It was found that the activated VPO catalyst provided exhibited high specific activity in the oxidation of *n*-butane to maleic anhydride (Ishimura et al., 2000).

Furthermore, an advantage of using this route is that sesquihydrate is capable of intercalated with dopants when using 1-butanol as reducing agent. Modified VPO catalyst often show high activity and selectivity to maleic anhydride (Ishimura et al., 2000).

2.4 Sonochemical Synthesis

Sonochemical synthesis refers to synthesising a compound or nanomaterial by using ultrasound irradiation. Ultrasound irradiation is believed to be able to improve the chemical reaction and mass transfer and the process is known as acoustic cavitation. By using ultrasound irradiation as a replacement for reflux method, the time required to prepare VPO catalyst decreases significantly but the activity of the catalyst is remained or even improved (Wong and Taufiq-Yap, 2011).

During ultrasound irradiation, the solution is subjected to compression and expansion periodically when the ultrasonic horn is vibrating at very high frequency, creating high and low pressure regions in the solution. This causes the dissolved air in the solution to diffuse and forms gas bubbles during the expansion or low pressure period. The gas bubbles will then be compressed by the compression or high pressure period as the compression and expansion is a periodical process. This cycle will continue until the gas bubbles is unable to withstand the external pressure of the gas bubble, causing it to collapse (Pokhrel et al., 2016).

When gas bubble collapse, two interesting physical phenomena will occur: creation of hotspot and shockwave. Hotspot refers to core of the collapsing gas bubble and it is reported by Pokhrel et al. (2016) that high-energy particle collision that can generate energy as high as 13 eV takes place in the hotspot. On the other hand,

implosion of gas bubble will create shock waves that is able to break up particles into tiny fragments which will further becomes the starting point of further acoustic cavitation process (Pokhrel et al., 2016).

2.5 Parameters of Vanadyl Pyrophosphate Catalyst

In addition to synthesising catalyst via different routes, various parameters can also affect the performance of VPO catalyst in the production of maleic anhydride. These parameters can be modified to improve the activity and selectivity of VPO catalyst. These parameters include:

- Calcination duration
- Calcination temperature
- Calcination environment
- Doped system
- P/V atomic ratio

2.5.1 Calcination Duration

Vanadyl phosphate sesquihydrate is a precursor to VPO catalyst. Calcination, a high temperature heat treatment is required to transform the precursor to the active component of VPO catalyst, vanadyl pyrophosphate.

Calcination duration is an important parameter because if calcination period is not sufficiently long, vanadyl phosphate sesquihydrate may not fully transform into vanadyl pyrophosphate. This can be observed from XRD results where the low intensity of the peak which signifies low crystallinity structure is obtained. On the other hand, if the calcination duration is too long, cracking of crystal structure of catalyst may occur. These problems can result in loss of surface area or catalyst deactivation (Taufiq-Yap et al., 2012).

The chemical stability of VPO catalyst is also associated with calcination duration. According to Albonetti et al. (1996), if vanadyl phosphate hemihydrate is calcined less than 100 hours, it is considered to be non-equilibrated catalyst which is often poorly crystallised, while equilibrated catalyst which is well crystallised is obtained if calcined for more than 1000 hours. Non-equilibrated catalyst has not achieved the minimum Gibbs energy yet, therefore, it is more active than equilibrated catalyst but selectivity to maleic anhydride from butane is poor (Albonetti et al., 1996).

2.5.2 Calcination Temperature

Similar to the calcination duration parameter, calcination temperature should also be optimum. Calcination at temperature that is too low reduce formation of the active phase vanadyl pyrophosphate. On the other hand, calcination at temperature that too high results in sintering of catalyst which decreases the surface area of the catalyst (Rajan et al., 2014).

The selectivity of VPO catalyst on oxidation of *n*-butane to maleic anhydride is dependent on the Lewis acidity of the catalyst. Based on an experiment conducted by Wang et al. (2010), they have concluded that calcination temperature is associated with the Lewis acidity of VPO catalyst.

2.5.3 Calcination Environment

According to IUPAC (2014)'s definition of calcination, calcination means heating in air or oxygen environment. However, this statement is not always true. Calcination environment can consist of inert or reactive gases. It has been found that calcination in the presence of mixture of butane and air can yield high performance VPO catalyst (Cheng and Wang, 1997).

Oxidizing strength of flowing gas is determined by the calcination environment. It was found that high oxidising strength can increase the vanadium valence of the used VPO catalyst and in turn, increasing the selectivity of *n*-butane to maleic anhydride. Besides that, oxidizing strength is also related to the surface structure of VPO catalyst. As the oxidising strength of flowing gas increases, the sizes of platelet increases as well, reducing the surface area. When using inert environment, VPO catalyst can formed in a short time but do not have good performance in oxidation of *n*-butane (Cheng and Wang, 1997).

When calcining non-promoted VPO catalysts, it is recommended to calcined in a more oxidising environment as non-promoted VPO is less active than promoted VPO. However, similar to other calcination parameters, oxidation strength should be intermediate as insufficient oxidation can lead to poor performance VPO while over-oxidation can decrease number of available V^{5+} on the surface of the catalyst and reduce conversion of *n*-butane (Cheng and Wang, 1997).

2.5.4 Doped System

Dopants is an impurity substance that is added on purpose into the compound that have an effect on the final catalyst either physical, chemical or both. Dopants can be classified into two categories: promoter and poison. Poison can have negative effect on the catalyst whereas promoter enhance the properties of the catalyst. VPO catalysts have been often doped with promoter in order to enhance their performance.

There are three ways in which a promoter can enhance the performance of VPO catalysts: structural, electronic or both. Structural promotional effects enhance the performance of VPO catalyst by increasing the surface area of the catalyst. The promoter prevents the formation of low surface area and inactive phases, $VO(H_2PO_4)_2$ by acting as a phosphorus scavenger. As pointed by Hutchings (1991), to achieve optimum performance, the vanadium to phosphorus to promoter atomic ratio should be within 1:1.15:0.15 to 1:1.20:0.20.

Electronic promotional effects on the other hand do not impose any structural effect on the catalyst due to low level of promoter in the catalyst structure. The promotional effects are achieved by a redox mechanism between the bulk and the surface of VPO catalyst (Hutchings, 1991).

Combination of both structural and electronic promotional effects is possible. Examples of promoter that exhibit such properties on VPO catalyst is cobalt, iron, aluminium and lithium. It is observed that VPO catalyst doped with lithium has increased ionic conductivity properties (Ballarini et al., 2006).

2.5.5 P/V Atomic Ratio

Phosphorus to vanadium, P/V atomic ratio is also another important parameter. It is found that a small change in P/V atomic ratio can results in different surface nature. When the P/V atomic ratio is equal to 1:1 and the reaction temperature is 340-400 °C, highly active phase α_1-$VOPO_4$ is formed over the surface of the catalyst. This highly active phase has very low selectivity to maleic anhydride. Only at 400-440 °C, the moderately active phase δ-$VOPO_4$ with good selectivity to maleic anhydride starts to form. When phosphorus is added in slight excess, the problem will be solved and δ-$VOPO_4$ forms at 340-440 °C. This is the reason why industrial VPO catalyst for maleic anhydride production always contains slight excess of phosphorus (Cavani et al., 2010).

According to Bartholomew and Farrauto (2005), the optimal P/V atomic ratio for VPO catalyst used in oxidation of *n*-butane should be 1.05. On the other hand,

Guliants et al. (1996) concluded that the best VPO catalyst should have P/V atomic ratio of 1.18. Thus, it is safe to conclude that the optimal P/V atomic ratio should be within the range of 1.05 to 1.18.

CHAPTER 3

METHODOLOGY

3.1 Materials

Chemicals involved in the experiment are listed as follows:

1. Vanadium pentoxide (Merck)
2. *Ortho*-Phosphoric acid
3. 1-butanol
4. Ammonium iron(II) sulphate
5. Sulphur acid
6. Potassium permanganate
7. Diphenylamine
8. Copper(II) nitrate
9. Cobalt(II) nitrate

The gases used are as follows:

1. 0.75 % *n*-butane in air
2. 99.99 % Purified Nitrogen
3. 99.99 % Purified Helium
4. Liquefied Nitrogen Gas

3.2 Methodology

In this research, performance of bulk VPO, VPO doped with copper, cobalt and both copper and cobalt was investigated based on their physical characteristics, chemical properties and reactivity. The VPO catalyst is prepared using sesquihydrate route with formation of dihydrate as intermediate product. The preparation procedures can be divided into three stages: preparation of dihydrate, preparation of sesquihydrate and calcination. Each stage is provided with detailed elaboration on steps taken to prepare the specimen.

3.3 Preparation of Vanadyl Phosphate Dihydrate Precursor

To prepare vanadyl phosphate dihydrate prevursor60.0 g of Vanadium pentoxide, V_2O_5 is added with 1440 mL of distilled water and 360 mL of *ortho*-phosphoric acid, *o*-H_3PO_4 in a 2000 mL beaker and stirred gently using a stirring rod. An ultrasound probe is then placed into the beaker to provide high intensity of ultrasonic irradiation to the solution. The ultrasound irradiation will be conducted for a duration of 4 hr. The resultant yellow precipitate is subjected to centrifugation to recover the yellow solids from the slurry. The yellow solid is then oven dried at 90 °C for 72 hr. The yellowish powder obtained is $VOPO_4 \cdot 2H_2O$.

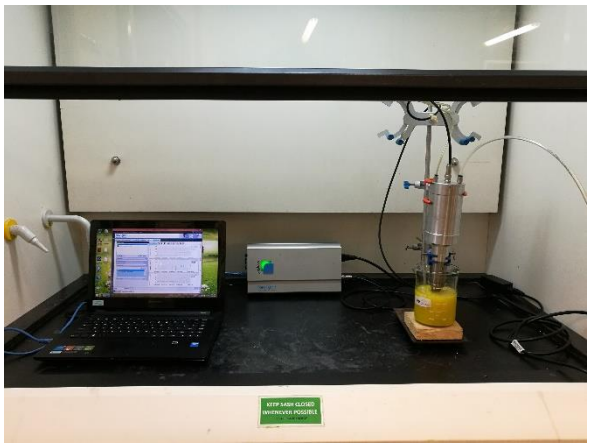

Figure 3.1: Set-up of Ultrasound Equipment

3.4 Preparation of Vanadyl Hydrogen Phosphate Sesquihydrate Precursor

In this stage, $VOHPO_4 \cdot 1.5H_2O$ will be synthesised by reducing $VOPO_4 \cdot 2H_2O$ in the presence of reducing agent, 1-butanol. Dopants are added during this stage as well according to the amount calculated. First, 15.0 g of $VOPO_4 \cdot 2H_2O$ from previous stage are added with 50 mL of 1-butanol and the required amount of dopants in a 100 mL beaker. The mixture is then stirred before subjected to ultrasound irradiation similar to previous stage for 4 hr. The resultant blue solids are then centrifuged out from the slurry and oven dried at 90 °C for 72 hr. The blue solids are $VOHPO_4 \cdot 1.5H_2O$ and are denoted as VPSBulk, VPSCo1%, VPSCu1% and VPSCu1%Co1%.

3.5 Calcination

In this stage, the doped $VOHPO_4 \cdot 1.5H_2O$ precursor is placed on 6 boats and a straight line is carved in at the center of each boat to increase the total surface area in contact

with gas. The boats are then arranged onto the holder and placed into a calcination reactor. Calcination process was conducted for a duration for 24 hr at 460 °C. Vanadyl pyrophosphate is then collected at the end of calcination process and are denoted as VPOBulk, VPOCo1%, VPOCu1% and VPOCu1%Co1%

3.6 Characterisation of Catalyst

Various characterisation methods were used to determine the physical, chemical and reactivity of the synthesised catalyst. The methods used in this research are: X-ray Diffraction Analysis (XRD), redox titration, Brunauer-Emmett-Teller Analysis (BET), Scanning Electron Microscope (SEM), Energy Dispersive X-Ray Spectrometry (EDX) and Temperature-Programmed Reduction (TPR).

3.6.1 X-ray Diffraction Analysis (XRD)

X-ray Diffraction Analysis (XRD) is a high precision x-ray crystallography technique that allows one to identify the phase composition present in the catalyst. The principle behind XRD is the interaction between x-ray and crystalline phase in the catalyst, which produce a diffraction pattern as shown in Figure 3.2. The relationship between angle of diffraction and atomic distance between crystal lattice can be related through Bragg Law (Equation 3.1). This technique is a non-destruction method (Stanjek and Häusler, 2004).

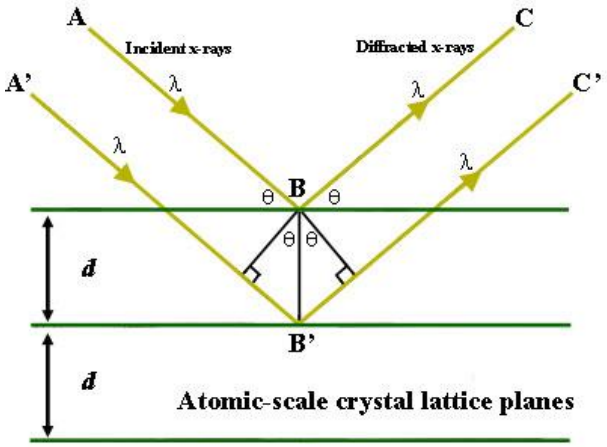

Figure 3.2: Schematics of the X-ray Diffraction.

$$2d\ sin\theta = n\lambda \quad (3.1)$$

X-ray diffractometer normally consists of sample holder, x-ray tube and detector which are mounted on mechanical rotating device known as goniometer. Two types of goniometer are available: θ:θ and θ:2θ. For θ:θ, the sample holder is fixed while x-ray tube and detector will move simultaneously to scan over range of θ specified. On the other hand, in a θ:2θ goniometer mechanical assembly, the x-ray tube is fixed while sample tube and detector moves. Sample tube rotates with θ while the detector moves at 2θ as shown in Figure 3.3. The diffracted signal is captured by detector and processed by a connected computer. The result is presented in a plot of diffracted intensities versus 2θ. By comparing the peak profile of the sample with database from Joint Committee on Powder Diffraction Standard (JCPDS), the phase composition can be determined (Stanjek and Häusler, 2004).

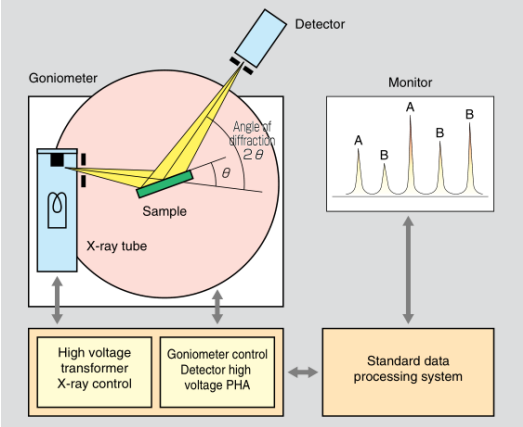

Figure 3.3: Flowchart on the Working Principle of XRD

Average crystallite size inside the particle can be calculated using Scherer's Equation (Equation 3.2) (Monshi et al., 2012).

$$L = \frac{K\lambda}{\beta cos\theta} \tag{3.2}$$

L = Average crystallite size (nm)

K = Shape factor of crystallite. About 0.89 for spherical crystals

λ = Wavelength of x-ray (nm)

β = Full Width at Half Maximum (rad)

θ = Diffraction angle (rad)

The XRD equipment used in this project is Shidmadzu 6000 XRD shown in Figure 3.4. Scanning rate of 1.2 ° per minute with CuKα radiation is used to analyse the sample. The range of scanning is from 2θ = 2 ° to 60 ° at ambient temperature and the peak profile of the sample is compared with the JCPDS PDF 1 database version 2.6.

Figure 3.4: Shidmadzu 6000 XRD

3.6.2 Redox Titration

Redox titration is a technique developed in 1982 by Niwa and Murakami to determine the average oxidation state of vanadium with the assumption that solution contains only V^{3+}, V^{4+} and V^{5+}. To be prepare the solution in this research, a known amount of catalyst is dissolved in sulphuric acid (2M). The solution is then titrated using potassium permanganate solution. This will cause V^{3+} and V^{4+} present in the solution to oxidise, forming V^{5+}. When the colour of the solution changes from greenish-blue to pink, end point is reached. The volume of potassium permanganate used was recorded as V_1 (Niwa and Murakami, 1982).

Next, the solution which now contains only V^{5+} was reduced by titrating with iron(II) ammonium sulphate. As the solution is colourless, diphenylamine was added to give the solution purple colour for ease of determining end point. When end point had reached, the solution is decolourised. At this stage, the solution now contains V^{4+}

and V^{5+}. The volume of iron(II) ammonium sulphate used was recorded as V_2 (Niwa and Murakami, 1982).

To determine the original amount of V^{5+} present in the solution, a fresh solution is prepared and titrated with iron(II) ammonium sulphate. Similarly, to indicate the end point, diphenylamine is used to give the solution purple colour. When the solution colour changes from violet to greenish-blue, end point has reached. This means that all V^{5+} have been reduced to V^{3+} and V^{4+}. The volume of iron(II) ammonium sulphate used was recorded as V_3 (Niwa and Murakami, 1982).

From these three steps, three equations can be obtained and used to determine the concentration of V^{3+}, V^{4+} and V^{5+} (Niwa and Murakami, 1982). A detailed derivation of the three equations are shown in Appendix B:

$$V^{3+} = 20(0.01)V_1 - 20(0.01)V_2 + 20(0.01)V_3 \quad (3.3)$$

$$V^{4+} = 40(0.01)V_2 - 40(0.01)V_3 - 20(0.01)V_1 \quad (3.4)$$

$$V^{5+} = 20(0.01)V_3 \quad (3.5)$$

After the concentration of V^{3+}, V^{4+} and V^{5+} is determined, the average oxidation state of vanadium, V_{AV} can be determined subsequently (Niwa and Murakami, 1982).

$$V_{AV} = \frac{5V^{4+} + 4V^{4+} + 3V^{3+}}{V^{5+} + V^{4+} + V^{3+}} \quad (3.6)$$

3.6.3 Scanning Electron Microscope (SEM)

Scanning Electron Microscope (SEM) is widely used to obtain information such as surface morphology and visual image of different phases composition present in the sample (Swapp, 2006). Hitachi S-3400N as shown in Figure 3.6 was used in this research. Prior to SEM analysis, the catalyst powder is required to be coated with electrically-conducting metal such gold. This is to increase the signal strength by increasing the amount of secondary electrons detectable in the SEM (Höflinger, 2013).

Figure 3.5: Hitachi S-3400

In SEM, a beam of electrons fired from the electron gun is focused onto the powder surface. Two types of signal will be produced as a result of interaction between electron beam and sample surface, namely secondary and backscattered electrons. Secondary electrons that produced from the inelastic collision between incident electrons with surface electrons are useful in imaging the morphology and topography of the samples. On the other hand, backscattered electrons that produced from the elastic collision between incident electrons with surface electrons are useful in distinguishing different phases with different molecular weight in the catalyst (Egerton, 2005). With the help of detectors in the SEM, signals are generated and the image of the SEM can be viewed through a monitor attached to the SEM. According to Cheney (2007), a working distance of 10 mm is generally used to produce an image with both decent depth of field and resolution.

In this project, Hitachi S-3400N SEM is used to analyse the sample surface morphology. Prior to SEM analysis, samples are required to be labelled accordingly and placed in the sputter coater to coat the sample with platinum. Then, the sample can now be placed into the SEM equipment. Before starting the analysis, the environment around the sample is vacuumed to remove the air molecules which can interfere with the observations under microscope. The test condition used to SEM is set at 15 kV and two pictures is taken for each sample at different magnification.

3.6.4 Energy Dispersive X-ray (EDX)

Energy Dispersive X-ray (EDX) is commonly used to identify the chemical composition of the catalyst qualitatively and quantitatively by analysing the x-rays

energy spectrum produced when an electron beam bombarded the catalyst surface (Goodge, 2005). EDX is usually coupled with SEM which shares the same electron gun for element mapping. Point analysis can also be carried out if X-ray detector is installed in the SEM machine (University of California, 2015).

When high-energy electron beam fired from electron gun interacts with the surface atoms of the catalyst, an electron is ejected from shell closest to the nucleus. This will cause movement of electrons from outer shell moves towards the inner shell to return the atom back to its stable, lowest energy state. The movement of electrons also releases X-ray, and depending which shell the electrons from, different radiation is released as shown in Figure 3.7 (Heath, 2015).

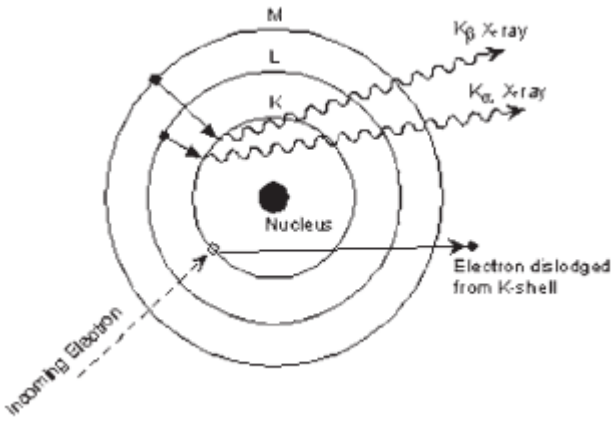

Figure 3.6: Different Radiation Emission During Excitation of Electrons

The resulting X-ray produced can be separated into characteristic x-rays of different elements into an energy spectrum. Since each element has their own unique energy spectrum, the composition can be identified accordingly. One of the limitations of EDX is the inability of detecting element lighter than beryllium (University of California, 2015).

The sample preparation steps for EDX is similar to SEM. The setting used for the test condition is 30 keV.

3.6.5 Temperature Programmed Reduction (TPR)

Temperature Programmed Reduction (TPR) is a relatively new thermoanalytical technique that has been widely used in chemical characterisation of catalyst. Temperature in TPR, as the name suggested can increase or decrease in a predetermined manner while at the same time the solid catalyst is being reduced by a

stream of diluted hydrogen gas. The gain of hydrogen by catalyst can be quantitatively determined by measuring the change in thermal conductivity of the inlet and outlet diluted hydrogen gas. The result is presented in the form of a plot of hydrogen consumed by catalyst versus the temperature. Each peak represents reduction process by a component in the catalyst. Chemical properties of the component can influence the position of the peak, while area under the peak represents the concentration of the component in the catalyst (Jones and McNicol, 1987).

TPR is carried out using Thermo Electron TPDRO 1100 shown in Figure 3.8 where initially, 0.02 g of catalyst is weighed into the reactor and connected to the preparation port. The catalyst is subjected a two-step pre-treatment process in which during the first step, a flow of purified nitrogen gas at 20 cm^3 min^{-1} is used to clean the catalyst for 5 minutes. The second step of pre-treatment involves increasing the temperature from room temperature to 473 K at 10 K min^{-1} for 45 min. The objective of pre-treatment is to remove any contaminant and moisture from the surface of catalyst.

Figure 3.7: Thermo Electron TPDRO 1100

After the completion of pre-treatment, reactor was switched to analysis port where a stream of 5.23 % hydrogen diluted in argon gas flows through the reactor. Temperature in the reactor was increased linearly from room temperature to 1173 K at 5 K min^{-1}. The hydrogen in the gas mixture reacts with the catalyst to form water and

removed from the reactor. Thermal conductivity detector measures the thermal conductivity difference and generates the results. Calculations required to analyse the result are shown in Appendix H and Appendix I

3.6.6 Inductively Coupled Plasma – Optical Emission Spectroscopy (ICP-OES)

Inductively Coupled Plasma – Optical Emission Spectroscopy (ICP-OES) is one of the most widely used tools to analyse the compositional information of the sample. This tool is applicable to solid, liquid and gaseous sample but solid samples are required to be dissolved in solution as it may clog the channel. Figure 3.9 shows the a typical ICP-OES instrument set up (Hou and Jones, 2000).

The sample is first introduced into the central plasma via a nebuliser which spray the sample solution into very fine particles. At the central of inductively coupled plasma, the temperature could reach up to 10000 K and the fine particles of sample solution is instantly vaporized. As the analyte elements are now free atoms in gaseous form, collision between the atoms can cause excitation of the atoms. When the excited species fall back to ground state, photon is released. Wavelength of the photons release by the element is unique to that element and be used as qualitative analysis of the sample. In addition, as the higher the number of photons produced, the higher concentration of the element present in the sample solution. Thus, ICP-OES can also be served as a quantitative analysis (Hou and Jones, 2000).

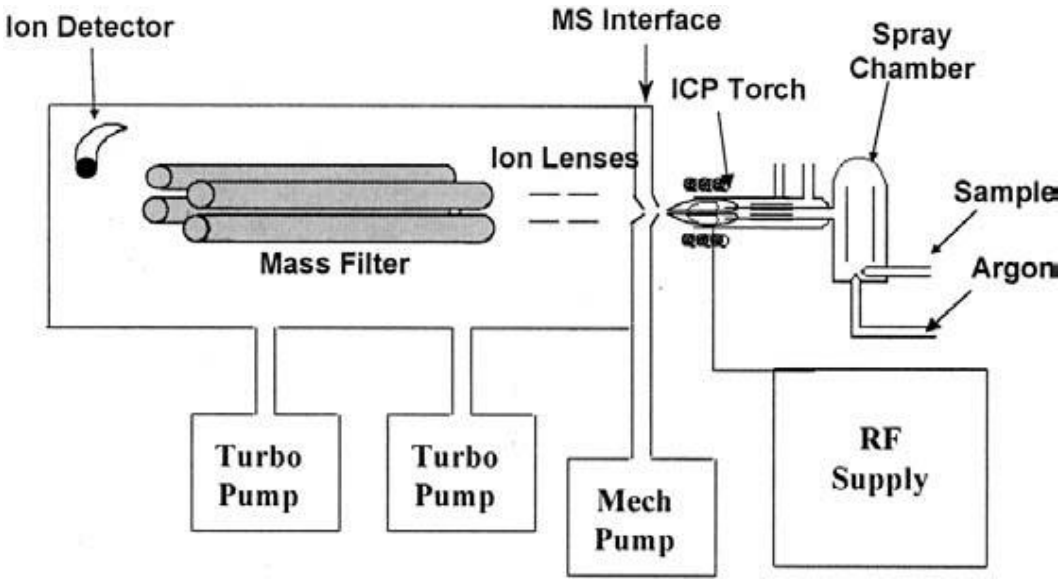

Figure 3.8: A typical ICP-OES Diagram

To carried out qualitative analysis using ICP-OES, it is necessary to run standards of the elements in interest before the sample analysis. The purpose for this step is to obtain a calibration curve and allow the unknown concentrations of the elements in the sample to be determined using the calibration curve.

In this research, standard solutions of V, P, Co, Cu were prepared with the concentration range from 5 ppm to 45 ppm. VPO catalyst were digested in 10 mL of HNO_3 to dissolve the solid completely. All the calculations and procedure involved is attached in Appendix D and Appendix E respectively. Perkin Elmer Optical Emission Spectrometer Optima 7000 DV as shown in Figure 3.10 is used in this research to carry out the ICP-OES analysis.

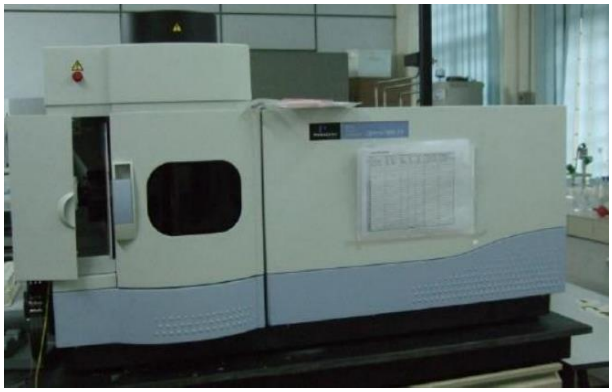

Figure 3.9: Perkin Elmer Optical Emission Spectrometer Optima 7000 DV

3.6.7 Fourier-Transform Infrared (FTIR)

Fourier-Transform Infrared (FTIR) analysis is commonly used to identify the type of functional groups and chemical bonding by monitoring the vibrational mode of the functional groups when exposed to infrared spectrum. Infrared spectrum ranges from wavelength of 700 nm to 1000000 nm but 2500 nm to 25000 nm is the most interesting range for chemical analysis. This is because most of the functional groups present in organic molecules fall within this range (Doyle, 1992).

The process of FTIR analysis is relatively direct. When the functional group or chemical bonds is exposed to infrared beam, portion of the energy is absorbed by the at a certain wavenumber and allow the functional group to vibrate in their vibrational mode. The amount of transmitted infrared beam is detected and the results is present in a plot of percent transmittance against wavenumber. Wavenumber is the inverse of wavelength (Doyle, 1992).

In this research, FTIR-ATR is used instead of traditional FTIR which uses potassium bromide (KBr) as the matrix material. The benefits of FTIR-ATR includes better results reproducibility, minimise sample preparation procedure that could cause spectral variation and faster sampling. Nicolet iS 10 as shown in Figure 3.11 is used in this research (Perkin Elmer, 2005).

Figure 3.10: Nicolet iS 10 FTIR Spectrometer

CHAPTER 4

RESULTS AND DISCUSSION

4.1 Introduction

The samples VPOBulk, VPOCo1%, VPOCu1% and VPOCu1%Co1% that were collected after the end of calcination process is subjected to various instrumental analyses to investigate the physical properties and chemical properties of the catalyst. These instrumental analyses include:

1) X-Ray Diffraction (XRD) Analysis
2) Fourier-Transform Infrared Spectroscopy (FTIR)
3) Scanning Electron Microscope (SEM)
4) Energy Dispersive X-ray Spectrometry (EDX)
5) Inductively Coupled Plasma - Optical Emission Spectroscopy (ICP-OES)
6) Redox Titration
7) Temperature-Programmed Reduction (TPR)

4.2 X-Ray Diffraction (XRD) Analysis

The XRD diffraction pattern of the four samples calcined at 460 °C in 0.75% *n*-butane in air mixture is shown in Figure 4.1. According to literature, the main characteristics peaks that are attributed to $(VO)_2P_2O_7$ phase is located at 2θ = 22.9 °, 28.4 ° and 29.9 ° (JCPDS File No. 34-1381).

However, from Figure 4.1, no peaks attributed to $(VO)_2P_2O_7$ phase can be observed. The XRD pattern of the all four VPO samples is actually similar to a typical XRD pattern of a highly amorphous solid. XRD analysis is not suitable to be used to analyse highly amorphous solid. This is because unlike crystalline solids where atoms are arranged in an orderly manner, atoms in amorphous solids are distributed randomly. When atoms are arranged in an orderly manner, X-rays will scatter in certain direction depending on which plane X-rays hit, resulting peaks with high intensity. However, in the case of highly amorphous solid, X-rays will scatter in many directions as the atoms are arranged randomly and results in a single wide peak over a large range of 2θ (Cullity, 1956).

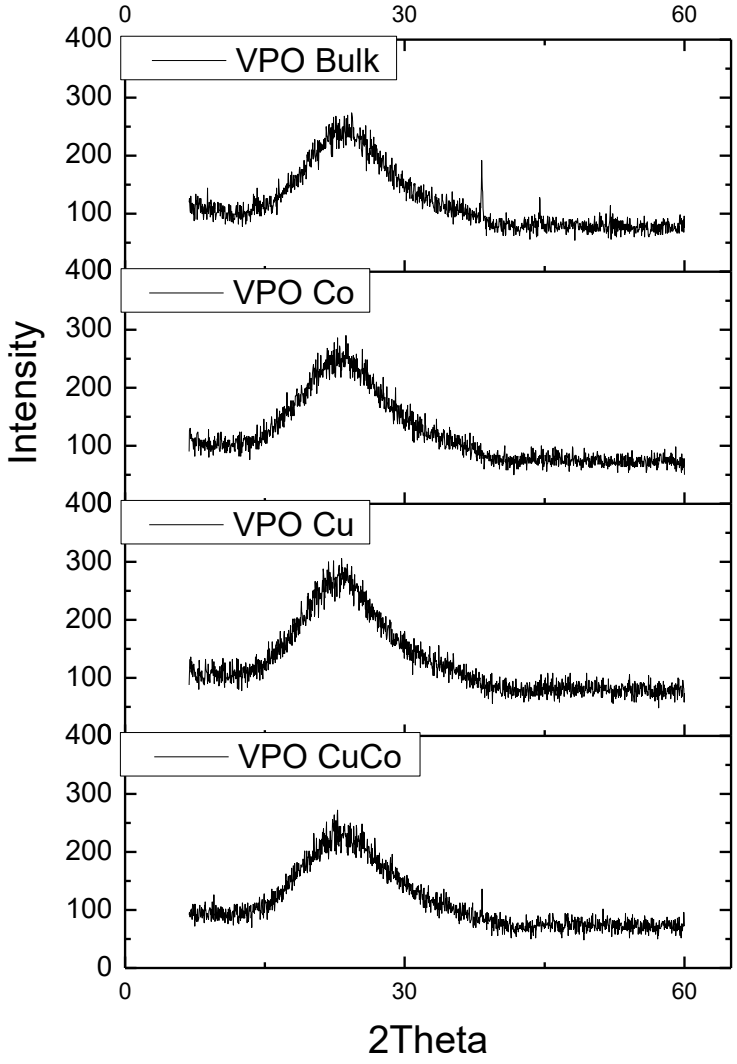

Figure 4.1: XRD Patterns of Undoped and Doped VPO Samples

Thus, based on Figure 4.1, it can be deduced that the VPOBulk, VPOCo1%, VPOCu1% and VPOCu1%Co1% produced are amorphous in nature. As XRD is unable to analyse amorphous solids, FTIR will be used instead to confirm the identity of the catalysts produced by determining the presence of characteristic bonds for VPO catalyst.

4.3 Fourier-Transform Infrared Spectroscopy (FTIR)

FTIR can be used to identify the molecular structure and type of chemical bonds presence due to their highly characteristic features. The FTIR spectra of the four samples are depicted in Figure 4.2. All the four VPO sample shows similar FTIR spectrum. The broad spectra band within the region of 2600-3600 cm^{-1} indicates the

presence of hydrogen bonded O - H groups while band at 1642 cm^{-1} is due to stretching mode of P-OH (Zhao et al., 2016).

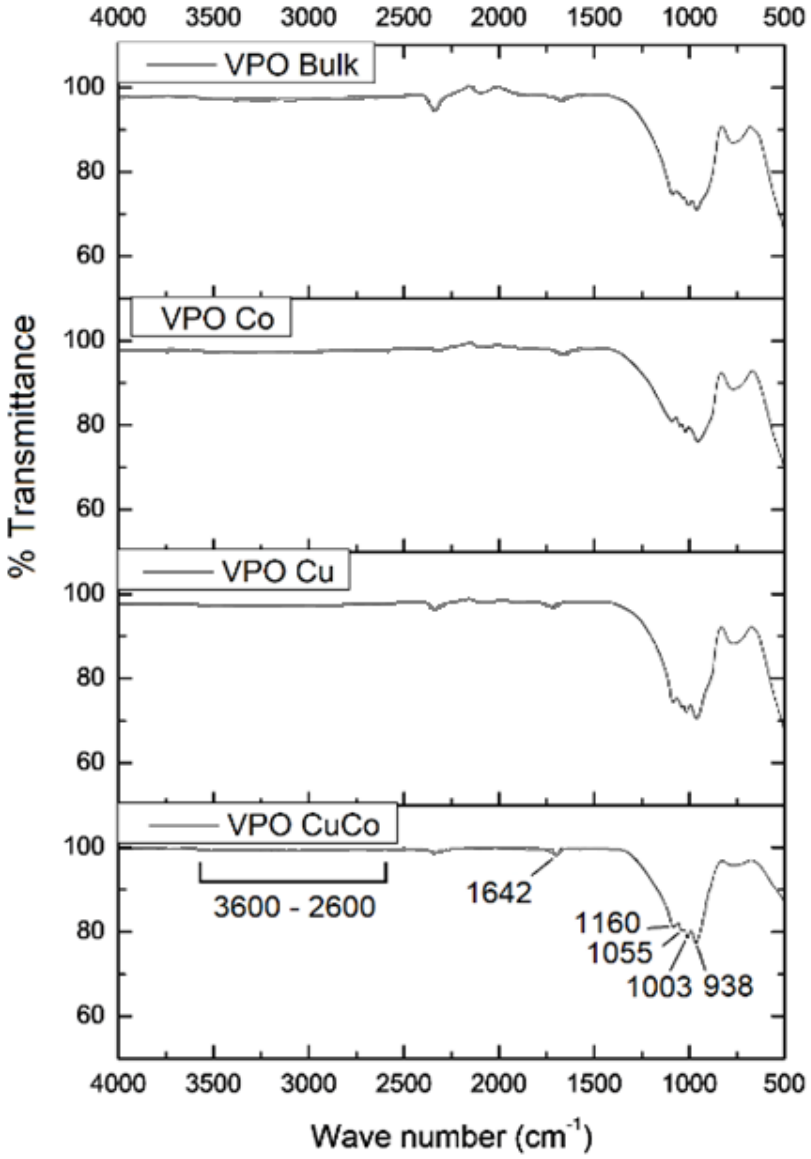

Figure 4.2: FTIR Spectra of VPO Samples Undoped and Doped

Spectra within the region of 900 – 1200 cm^{-1} represents the P - O and V = O groups. To be in precise, the band in 1160 and 1055 cm^{-1} is due to bending of PO_3, the band in 1003 cm^{-1} is due to stretching of V = O and the band in 938 cm^{-1} is due to stretching of V - OH. The band located at 642 cm^{-1} on the other hand, is due to deformation vibrations of phosphate tetrahedral (Zhao et al., 2016).

As all the IR spectra indicates the presence of P - O and V = O bonding in the samples, it can be affirmed that the VPOBulk, VPOCo1%, VPOCu1% and VPOCu1%Co1% contained active phase of $(VO)_2P_2O_7$ in the samples.

4.4 Scanning Electron Microscope (SEM)

The surface morphologies of VPOBulk, VPOCo1%, VPOCu1% and VPOCu1%Co1% catalysts are shown in Figure 4.3(a)-(d). It can be seen that all the catalysts have a different shape and sizes due to presence of dopant. Undoped VPO, as can be observed from Figure 4.3(a) has a blocky crystals structure due to the agglomeration of particles. These agglomerates of VPO sample often expose the (1 0 0) crystal plane.

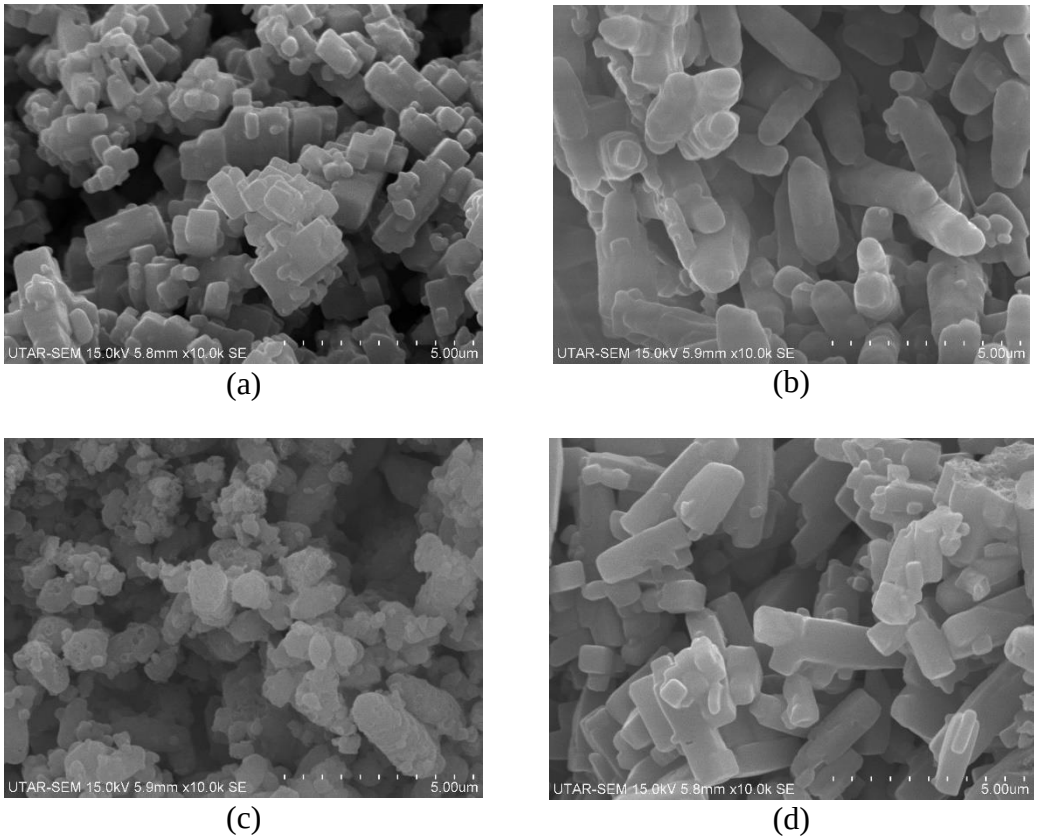

Figure 4.3: SEM Micrographs of (a) VPOBulk (b) VPOCo1% (c) VPOCu1% (d) VPOCu1%Co1% at ×10000 magnification

Figure 4.3(b) to (d) depicts the surface morphologies for various doped VPO catalyst. VPO doped with 1% of cobalt has a rod-like crystals structure while VPO doped with 1% of copper has a grain-like crystal structure. However, when both cobalt and copper are added into VPO catalyst, it can be observed that the promotional effect

from cobalt is the more dominant compared to copper as VPOCu1%Co1% crystal shape (Figure 4.3(d)) is more similar to rod-like crystal structure.

All the doped catalysts have an average crystallite size of 10 µm while undoped catalyst has an average crystallite size of 20 µm. Crystallite size is known to be inversely proportional to the surface area and the activity of the catalyst. A smaller crystallite size can increase the specific surface area of the catalyst and enhances the catalytic performance of the catalyst. This is in agreement with literature findings where copper and cobalt both increase the specific surface area on the catalyst (Hutchings and Higgins, 1996).

4.5 Energy Dispersive X-ray Spectrometry (EDX)

The compositional data for the VPO samples obtained from EDX is tabulated in Table 4.1. Accuracy of quantitative analysis using EDX can be affected when the sample has irregular sample surface and non-homogeneous. This is because to produce accurate quantitative results, all the X-ray produced from the interaction between the electron beam and the particles must be detected. When the surface is coarse or non-homogenous, the X-ray produced will be interfered and produce inconsistent reading.

Table 4.1: Compositions of VPO Samples and the Average P/V Atomic Ratio

Catalyst	P_{avg} (At. %)	V_{avg} (At. %)	O_{avg} (At. %)	Co_{avg} (At. %)	Cu_{avg} (At. %)	Average P/V
VPOBulk	47.16	37.38	15.56	-	-	1.2619
VPOCo1%	38.56	35.21	25.49	0.74	-	1.0951
VPOCu1%	41.14	39.89	18.28	-	0.69	1.0313
VPOCu1%Co1%	40.92	37.93	19.57	0.67	0.92	1.0788

To improve the accuracy of result obtained, elementary compositions at three points are analysed to obtain an average value. Average P/V atomic ratio is then calculated by dividing P_{avg} with V_{avg}.

Based on literature, the optimal range of the P/V atomic ratio should be within the range of 1.00 – 1.20 (Gulliants, 1996). As can be seen in Table 4.1, the P/V atomic ratio of undoped catalyst is 1.2619 which is above the optimal range. On the other hand, the incorporation of dopants in VPOCo1%, VPOCu1% and VPOCu1%Co1%

has greatly reduced the P/V atomic ratio of VPO catalyst where all doped catalysts fall within the optimal range of P/V atomic ratio.

It was suggested that a slight excess of P can promote the stabilisation of V^{4+} that is responsible for the poor selectivity and high activity of catalyst (Taufiq-Yap et al., 2011). However, when the P/V atomic ratio is too high, the crystalline phase of the catalyst will reduce while formation of amorphous $VOPO_4$ phases will increase (Guliants, Benziger, S. Sundaresan, et al., 1996).

The average P/V atomic ratio for VPO catalyst doped with 1 % Copper and 1 % Cobalt is 1.0788. This value lies on the in between the P/V atomic ratio of VPOCo1% and VPOCu.1% but closer towards the VPOCo1% in which the P/V atomic ratio is 1.0951. This is due to more dominant promotional effect as discussed in SEM analysis where cobalt has a more prominent promotional effect on VPO catalyst than copper.

As EDX analysis is a surface analysis technique where only x-ray generated from the surface atom up to a few microns thick can be detected. This may reduce the actual amount of phosphorous detectable by EDX analysis.

4.6 Inductively Coupled Plasma - Optical Emission Spectroscopy (ICP-OES)

To support the results obtained from EDX analysis, ICP-OES is carried out to analyse the elementary composition of the VPO samples undoped and doped. The results obtained from ICP-OES is shown in Table 4.2. To improve the accuracy of the results, each element is analysed three times by the ICP-OES and the average concentration of the element is calculated.

Table 4.2: P/V Atomic Ratio from ICP-OES

Catalyst	P_{avg} (mg/L)	V_{avg} (mg/L)	Co_{avg} (mg/L)	Cu_{avg} (mg/L)	Average P/V
VPOBulk	3.380	5.121	-	-	1.0855
VPOCo1%	5.919	9.589	0.084	-	1.0153
VPOCu1%	41.14	39.89	-	0.157	0.9342
VPOCu1%Co1%	40.92	37.93	0.068	0.076	0.9577

Based on Table 4.2, it can be observed that VPOBulk has a higher P/V atomic ratio, followed by VPOCo1%, VPOCu1%Co1% and lastly VPOCu1%. The trend is in agreement with the result obtained from EDX analysis. Thus, it can be said the cobalt and copper dopant can reduce the average P/V atomic ratio in the VPO catalyst.

However, all the VPO samples have a much lower average P/V atomic ratio in general compared to the results obtained from EDX analysis. Not only that, all the doped catalysts even fall out of the optimal range as proposed by Guliants et al. (1996). The P/V atomic ratio can be related to the oxidation of $(VO)_2P_2O_7$. A slightly high P/V atomic ratio can stabilize $(VO)_2P_2O_7$ phases and prevent oxidation of the phases to V^{5+} but when P/V atomic ratio is too high, amorphous phases $VOPO_4$ will form. On the other hand, a low P/V atomic ratio is unable to limit the oxidation of $(VO)_2P_2O_7$ phases to $VOPO_4$ as well. V^{5+} is present in $VOPO_4$ phase and is only desired in VPO catalyst in a small quantity compared to V^{4+} as V^{5+} can decrease the activity of the catalyst and increase the selectivity (Guliants et al., 1996).

As the average P/V atomic ratio found in EDX are greater than the average P/V atomic ratio determined from ICP-OES, it can be deduced that most phosphorous is segregated near the surface of VPO catalyst due to presence of an amorphous metaphosphate phase near the surface as pointed out by Ruitenbeek (1999). However, the formation of this metaphosphate phase should be minimum as the P/V ratio found in EDX is still relatively small compared to the literature findings in which the P/V atomic ratio is 4.0. Moreover, the results from ICP-OES can also be considered as an overall composition ratio that include the catalyst bulk and catalyst surface as well.

4.7 Redox Titration

Redox titration is carried out to determine the average oxidation number of vanadium at the amount of V^{4+} and V^{5+} present in the VPO catalyst. V_{AV} is calculated from the data obtained in redox titration while V^{4+} and V^{5+} can be determined from V_{AV}. Table 4.3 shows all the results calculated.

From the Table 4.3, it can be observed that the average oxidation number of VPOBulk, VPOCo1%, VPOCu1% and VPOCu1%Co1% are 4.2044, 4.1803, 4.2454 and 4.3054 respectively. An interesting difference can be observed where the presence of cobalt dopant decreases the average oxidation number of the VPO catalyst while the addition of copper dopant increases the average oxidation number of the VPO

catalyst. This former is in fact in agreement with the result obtained by Cornaglia et al. (2003) where the researchers found that cobalt dopant can reduce the average oxidation number of the VPO catalyst by promoting phosphorous enrichment and limit the oxidation of V^{4+}.

Table 4.3: Average Oxidation Number of Vanadium from Redox Titration

Catalyst	Average oxidation number of vanadium		
	V^{4+} (%)	V^{5+} (%)	V_{AV}
VPOBulk	79.56	20.44	4.2044
VPOCo1%	81.94	18.06	4.1803
VPOCu1%	75.46	24.54	4.2454
VPOCu1%Co1%	69.46	30.54	4.3054

On the other hand, the latter, where addition of copper dopant increase the average oxidation number of VPO catalyst can also observed in EDX analysis and ICP-OES analysis where VPOCu1% has the lowest P/V ratio among the four samples. Low P/V atomic ratio will increase the formation of $VOPO_4$ phases which in turn increase the V^{5+} present in the VPO catalyst. Thus it can be concluded that addition of cobalt decreases the average oxidation number while addition of copper increases the average oxidation number in a VPO catalyst.

When comparing the average oxidation number of VPOCu1%Co1% with other VPO samples, it was found that the average oxidation number of VPOCu1%Co1% was higher than the other samples. This may be the result of the synergistic effect between cobalt and copper dopant where presence of cobalt enhances the promotional effect of copper dopant. A higher average oxidation number can be translated to higher number of V^{5+} present in the VPO catalyst. As high number of V^{5+} can decrease the activity of VPO catalyst significantly albeit it increases of selectivity towards oxidation of *n*-butane to maleic anhydride, it is undesired in the industry.

4.8 Temperature-Programmed Reduction (TPR)

TPR is used to analyse the redox properties of VPO catalyst by flowing reducing agent, H_2 diluted in inert gas over the catalyst. Before subjecting the sample for TPR analysis, pre-treatment of the catalyst is carried out to fully oxidised the catalyst and remove

any impurities on the catalyst surface. Figure 4.4 depicts the TPR profile for VPOBulk, VPOCo1%, VPOCu1% and VPOCu1%Co1%. By using the data obtained from Figure 4.4, reduction activation energy (E_R) and total amount of oxygen removed from the VPOs catalysts is calculated and tabulated in Table 4.4.

Table 4.4: Total amount of O_2 removed from the VPOs catalysts.

Catalyst	Peak	T_m (K)	E_R (kJ/mol)	Amount of oxygen removed (mol/g)	Amount of oxygen removed (atom/g)	Total oxygen removal (atom/g)
VPOBulk	1	703	108.0824	7.67×10^{-5}	4.62×10^{19}	**1.48×10^{20}**
	2	932	143.2899	1.69×10^{-4}	1.02×10^{20}	
VPOCo1%	1	689	105.9300	7.16×10^{-6}	4.16×10^{18}	**1.24×10^{20}**
	2	948	145.7498	2.00×10^{-4}	1.20×10^{20}	
VPOCu1%	1	697	107.1599	6.91×10^{-6}	4.16×10^{18}	**1.17×10^{20}**
	2	918	141.1374	1.88×10^{-4}	1.13×10^{20}	
VPOCu1% Co1%	1	679	104.3925	5.86×10^{-6}	3.53×10^{18}	**1.21×10^{20}**
	2	923	141.9062	1.95×10^{-4}	1.18×10^{20}	

As can be seen from Figure 4.4, all VPOs catalysts showed two peaks in the TPR profile while the latter peak has a higher amount of oxygen removed from catalyst. The temperature at which a peak is located, temperature maxima is relatively similarly for all the VPOs catalyst. It can be deduced adding cobalt, copper and both cobalt and copper at the same time do not affect the temperature at which oxygen starts to remove from the catalyst.

Different oxygen species is removed from the VPO catalyst at different peaks. The first peak will correspond to the release of selective oxygen species, O^{2-} from the V^{5+} phase. On the other hand, the second peak will correspond to the release of unselective oxygen species, O^- from the V^{4+} phase (Taufiq-Yap et al., 1997). As the V^{4+} constitute a larger portion in the VPO catalyst, more oxygen is removed during the second peak compared to the first peak. Figure 4.5 shows the amount oxygen removed from V^{4+} and V^{5+} respectively. It can be observed all four samples shows

similar trend where V^{4+} phases release more oxygen than V^{5+} phases. This result is in consistent with the findings from redox titration where the percentage of V^{4+} phases roughly range from 69.46 % to 81.94 %.

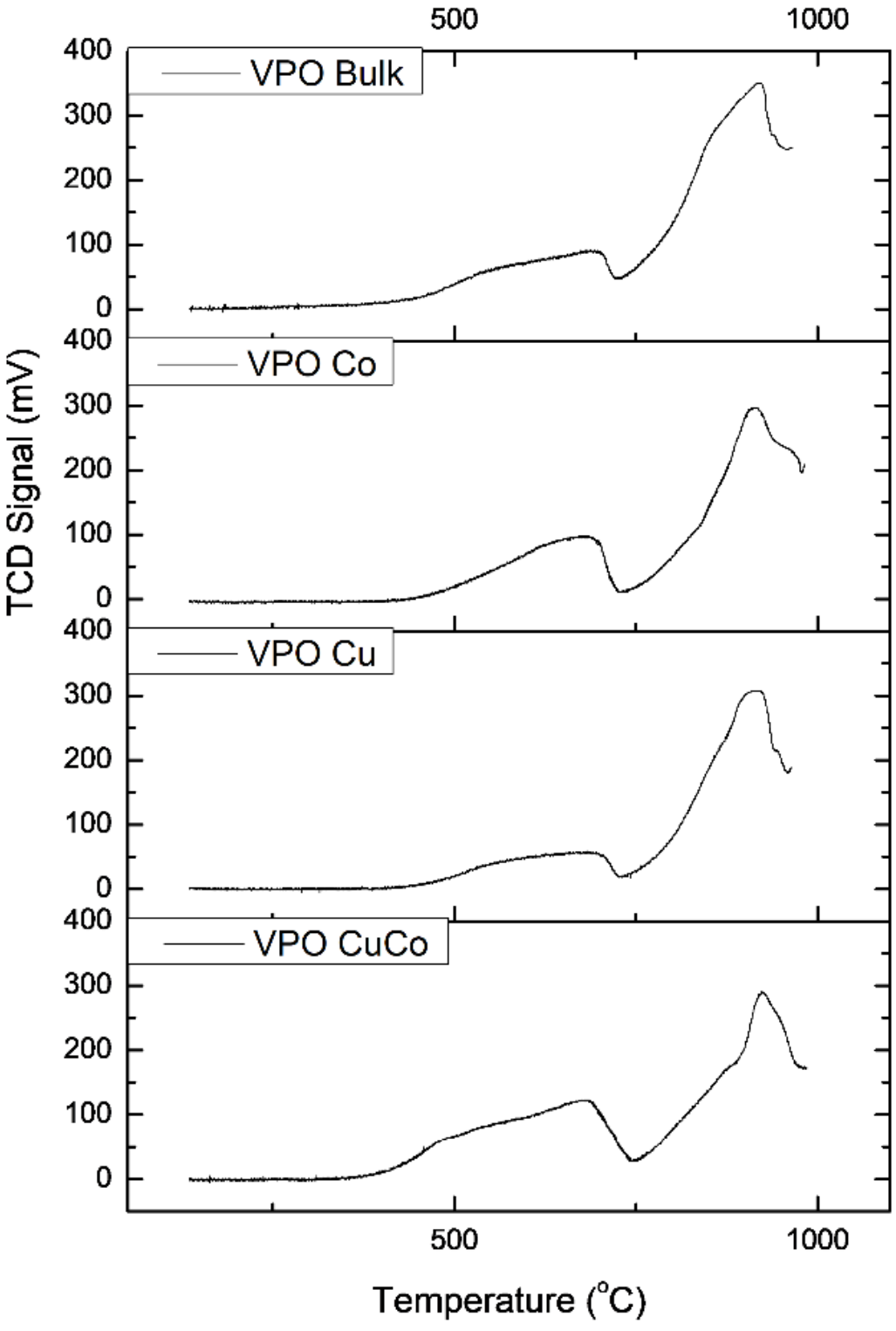

Figure 4.4: TPR Profiles of VPOs Catalysts

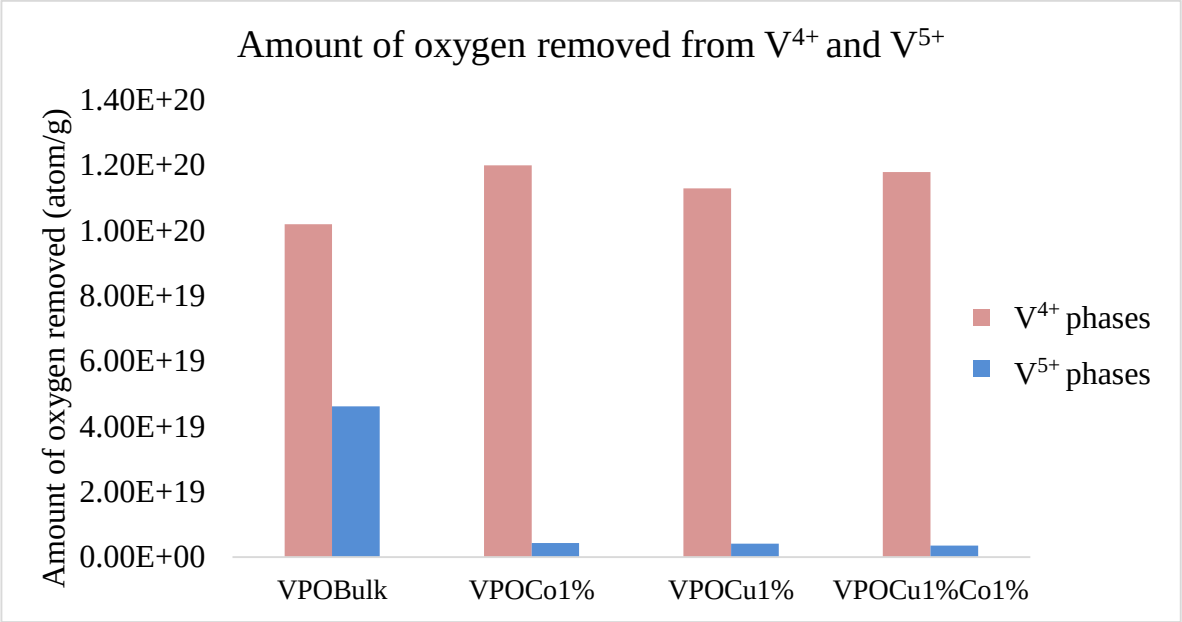

Figure 4.5: Comparison of amount of oxygen removed from catalyst between V^{4+} and V^{5+} phases

In terms of total oxygen removed from the VPO catalyst, VPOBulk has the highest amount of oxygen removed followed by VPOCo1%, VPOCu1%Co1% and VPOCu1%. This may be related to the surface morphology of doped catalyst where all three doped catalyst has rod-like structure in SEM which has lower specific surface area compared to VPOBulk which has a blocky structure.

Based on Table 4.4, it can also be seen that different dopants have different effect on the reduction activation energy of VPO catalyst. As reduction activation energy represent the minimum energy required for the redox mechanism to take place in the VPO catalyst, a lower reduction activation energy is often desired. Addition of cobalt is found to decrease the E_R of V^{4+} phases but increase the E_R of V^{5+} phases while addition of copper will reduce E_R of both V^{4+} and V^{5+} phases. On the other hand, the E_R for VPOCu1%Co1% is reduced compared the VPOBulk and this may be due to the synergistic effect between cobalt and copper dopant.

CHAPTER 5

CONCLUSION AND RECOMMENDATIONS

5.1 Conclusion

In this research, preparation of vanadyl phosphate dihydrate precursor is conducted by ultrasound irradiation for 1 hour followed by preparation of vanadyl phosphate sesquihydrate precursor which subjected to ultrasound irradiation for 4 hours. The sesquihydrate precursor is then calcined at 460 °C for 24 hours. Vanadyl pyrophosphate catalyst obtained at the end of calcination is characterised using various techniques.

From XRD, it was found that all the four VPOs catalyst has amorphous structure. FTIR is used instead to identify the identity of the catalyst by determining the bond present. The presence of P-O and V=O bonding shows that the identity of the catalyst is indeed VPO catalyst. Thus, it can be concluded that bulk VPO catalyst, Cu-doped VPO catalysts, Co-doped VPO catalysts and Cu-Co doped VPO catalysts were successfully synthesised using sonochemical technique.

The P/V atomic ratio from for all doped catalysts are found lower than undoped catalysts but within the optimal range in EDX analysis. Cobalt has a more prominent promotional effect on VPO catalyst than copper as bi-metallic doped VPO catalyst has an intermediate atomic P/V ratio but the value is closer to cobalt doped VPO. This effect can also be observed in SEM micrographs where cobalt distinctive rod-like shape is present in the bi-metallic doped VPO catalyst. The trend obtained ICP-OES is in agreement with EDX analysis, but the value is lower in general. This is due to formation of small amount of metaphosphate phase in the VPO catalyst.

In addition, it was found from redox titration analysis that addition of cobalt into the VPO catalyst can decrease the average oxidation number of vanadium and this is in agreement with Cornaglia et al. (2003) findings. Presence of cobalt dopant will promote phosphorus enrichment and limit the oxidation of V^{4+}. On the other hand, addition of copper increases the average oxidation number of vanadium as copper doped VPO catalyst has a lower P/V atomic ratio which allows more formation of $VOPO_4$ phases. The results from redox titration is supported by TPR profile of the catalyst. It can be seen that cobalt doped VPO has more oxygen species from the V^{4+}

phase than the copper doped VPO because higher amount of V^{4+} phase is present in cobalt doped VPO catalyst.

The synergistic effect between cobalt and copper dopants can be observed in both redox titration and TPR analysis. In redox titration, cobalt dopant enhances the promotional effect of copper dopant, producing a bi-metallic doped VPO catalyst with higher percentage of V^{5+} present in the catalyst. From TPR analysis, it was found that the reduction activation energy is reduced and this may be related to the synergistic effect between cobalt and copper dopant in VPO catalyst.

5.2 Recommendations

For further research:

1) To understand the catalyst produced better, the catalyst should be analysed using a catalytic reactor to obtain information on actual yield of maleic anhydride. Yield is one of the key factor to select the optimal catalyst.
2) Different routes can be used to synthesise VPO catalyst, including hemihydrate and organic route. Research should be done to distinguish the route which is most suitable to produce catalyst.

REFERENCES

Al-Otaibi, R.L., 2010. *Preparation and Characterisation of Vanadium Phosphorus Oxide Catalysts for Butane Oxidation to Maleic Anhydride*. University of Cardiff.

Albonetti, S. et al., 1996. A Comparison of the Reactivity of "Nonequilibrated" and "Equilibrated" V–P–O Catalysts: Structural Evolution, Surface Characterization, and Reactivity in the Selective Oxidation of n-Butane andn-Pentane. *Journal of Catalysis*, 160(1), pp.52–64.

Ballarini, N. et al., 2006. VPO catalyst for n-butane oxidation to maleic anhydride: A goal achieved, or a still open challenge? *Topics in Catalysis*, 38(1–3), pp.147–156.

Bartholomew, C.H. and Farrauto, R.J., 2005. *Fundamentals of Industrial Catalytic Processes* 2nd ed., John Wiley & Sons, Inc., Hoboken, NJ, USA.

Benziger, J.B., Guliants, V. and Sundaresan, S., 1997. New precursors to vanadium phosphorus oxide catalysts. *Catalysis Today*, 33(1–3), pp.49–56.

Brunauer, S., Emmett, P.H. and Teller, E., 1938. Adsorption of Gases in Multimolecular Layers. *Journal of the American Chemical Society*, 60(2), pp.309–319. Available at: http://pubs.acs.org/doi/abs/10.1021/ja01269a023.

Cavani, F. et al., 2010. Surface dynamics of a vanadyl pyrophosphate catalyst for n-butane oxidation to maleic anhydride: An in situ Raman and reactivity study of the effect of the P/V atomic ratio. *Chemistry - A European Journal*, 16(5), pp.1646–1655.

Cheney, B., 2007. Introduction to Scanning Electron Microscopy. , 29(2), pp.29–36. Available at: http://www.ncbi.nlm.nih.gov/pubmed/3313016.

Cheng, W.-H. and Wang, W., 1997. Effect of calcination environment on the selective oxidation of n-butane to maleic anhydride over promoted and unpromoted VPO catalysts. *Applied Catalysis A: General*, 156(1), pp.57–69.

Chorendorff, I. and Niemantsverdriet, J.W., 2003. *Concepts o Modern Catalysis and Kinetics* 2nd ed., Wiley-VCH, Weiheim.

Cole-Hamilton, D.J., 2003. Homogeneous Catalysis--New Approaches to Catalyst Separation, Recovery, and Recycling. *Science*, 299(1702). Available at: http://www.sciencemag.org/cgi/doi/10.1126/science.1081881.

Cornaglia, L. et al., 2003. The beneficial effect of cobalt on VPO catalysts. *Catalysis Today*, 78(1–4 SPEC.), pp.291–301.

Cullity, B.D., 1956. *Elements of X-ray Diffraction* First., Addison-Wesley Publishing Company, Inc., Massachusetts.

Dollimore, D., Spooner, P. and Turner, A., 1976. The BET method of analysis of gas adsoprtion and its relevance to the calculation of surface area. *Surface Technology*, 4, pp.121–160.

Doyle, W.M., 1992. Principles and applications of Fourier transform infrared (FTIR) process analysis. *Process Control and Quality*, 2, pp.11–41.

Egerton, R.F., 2005. *Physical principles of electron microscopy: An introduction to TEM, SEM, and AEM*, Springer, United States.

Farrauto, R.J., Dozario, L. and Bartholomew, C.H., 2016. *Introduction to Catalysis and Industrial Catalytic Processes* 1st ed., John Wiley & Sons, Inc., United States.

Goodge, J., 2005, *Energy-Dispersive X-Ray Spectroscopy (EDS)* [Online]. Available at: http://serc.carleton.edu/research_education/geochemsheets/eds.html.

Guliants, V.V., Benziger, J.B., Sundaresan, S., et al., 1996. The effect of the phase composition of model VPO catalysts for partial oxidation of n-butane. *Catalysis Today*, 28(4), pp.275–295.

Haynes, W.M., 2013. *CRC Handbook of Chemistry and Physics* 94th ed., CRC Press, Florida.

Heath, J., 2015. Energy Dispersive Spectroscopy. *Essential Knowledge Briefings*, (2), p.32.

Höflinger, G., 2013, *Brief Introduction to Coating Technology for Electron Microscopy* [Online]. Available at: http://www.leica-microsystems.com/science-lab/brief-introduction-to-coating-technology-for-electron-microscopy/.

Hou, X. and Jones, B.T., 2000. *Inductively Coupled Plasma-Optical Emission Spectroscopy*, John Wiley & Sons, Inc., Chichester.

Hutchings, G.J., 1991. Effect of promoters and reactant concentration on the selective oxidation of n-butane to maleic anhydride using vanadium phosphorus oxide catalysts. *Applied Catalysis*, 72(1), pp.1–32.

Hutchings, G.J. and Higgins, R., 1996. Effect of promoters on the selective oxidation of n-butane with vanadium-phosphorus oxide catalysts. *Journal of Catalysis*, 162(2), pp.153–168.

Hwang, N. and Barron, a. R., 2011. BET Surface Area Analysis of Nanoparticles. , 1, pp.1–11.

Ishimura, T., Sugiyama, S. and Hayashi, H., 2000. Vanadyl hydrogenphosphate sesquihydrate as a precursor for preparation of (VO)2P2O7 and cobalt-incorporated catalysts. *Journal of Molecular Catalysis A: Chemical*, 158(2), pp.559–565. Available at: http://linkinghub.elsevier.com/retrieve/pii/S138111690000145X.

IUPAC, 2014. *Compendium of Chemical Terminology Gold Book* 2.3.3., IUPAC.

Jackson, S.D. and Hargreaves, J.S.J., 2009. *Metal Oxide Catalysis Vol 1* 1st ed. Jackson, S.D. and Hargreaves, J.S.J., (eds.), Wiley-VCH, Weiheim.

Johannes, T.W., Simurdiak, M.R. and Zhao, H., 2006. Biocatalysis. *Encyclopedia of Chemical Processing*, pp.101–110.

Jones, A. and McNicol, B.D., 1987. *Temperature Programmed Reduction for Solid Materials Characterization in Chemical Industries*, New York.

Leong, L.K., Chin, K.S. and Taufiq-Yap, Y.H., 2011. The effect of Bi promoter on vanadium phosphate catalysts synthesized via sesquihydrate route. *Catalysis Today*, 164(1), pp.341–346. Available at: http://dx.doi.org/10.1016/j.cattod.2010.10.029.

Mazur, L., 2001. Catalysts - Real-life applications. *Science Clarified: Real-Life Chemistry*, 1. Available at: http://www.scienceclarified.com/everyday/Real-Life-Chemistry-Vol-2/Catalysts-Real-life-applications.html [Accessed: 23 March 2017].

Monshi, A., Foroughi, M.R. and Monshi, M.R., 2012. Modified Scherrer equation to estimate more accurately nano-crystallite size using XRD. *World J. Nano Sci. Eng.*, 2(3), p.154.

Musa, O.M., 2016. *Handbook of Maleic Anhydride Based Materials* Musa, O.M., (ed.), Springer, New Jersey.

Niwa, M. and Murakami, Y., 1982. Mechanism of Ammoxidation of Toluene. *Journal of Catalysis*, (76), pp.9–16.

Perkin Elmer, 2005. FT-IR Spectroscopy Attenuated Total Reflectance (ATR). *Perkin Elmer Life and Analytical Sciences*, pp.1–5. Available at: http://www.utsc.utoronto.ca/~traceslab/ATR_FTIR.pdf.

Pokhrel, N., Vabbina, P.K. and Pala, N., 2016. Sonochemistry: Science and Engineering. *Ultrasonics Sonochemistry*, 29(July 2016), pp.104–128. Available at: http://dx.doi.org/10.1016/j.ultsonch.2015.07.023.

Rajan, N.P., Rao, G.S., Pavankumar, V. and Chary, K.V.R., 2014. Vapour phase dehydration of glycerol to acrolein over NbOPO4 catalysts. *Journal of Chemical Technology and Biotechnology*, 89(12), pp.1890–1897.

Ruitenbeek, M., 1999. Determination of The Surface Composition of V-P-O Catalysts. *X Ray Photoelectron Spectroscopy*, pp.41–56.

Stanjek, H. and Häusler, W., 2004. Introduction To Powder/ Polycrystalline Diffraction. *Hyperfine Interactions*, 154, pp.107–119.

Swapp, S., 2006, *Scanning Electron Microscopy (SEM)* [Online]. Available at: http://serc.carleton.edu/research_education/geochemsheets/techniques/SEM.html.

Taufiq-Yap, Y.H. et al., 2012. Effect of different calcination duration on physicochemical properties of vanadium phosphate catalysts. *E-Journal of Chemistry*, 9(3), pp.1440–1448.

Taufiq-Yap, Y.H., Nurul Suziana, N.M. and Hussein, M.Z., 2011. Influences of the

various metal dopants for the nanosized vanadium phosphate catalysts. *Catalysis Letters*, 141(1), pp.136–148.

Taufiq-Yap, Y.H., Sakakini, B.H. and Waugh, K.C., 1997. Investigation of the nature of the oxidant (selective and unselective) in/on a vanadyl pyrophosphate catalyst. *Catalysis Letters*, 48(1/2), pp.105–110.

University of California, 2015. Introduction to Energy Dispersive X-ray Spectrometry (EDS). , pp.1–12. Available at: http://cfamm.ucr.edu/documents/eds-intro.pdf.

Védrine, J.C., Hutchings, G.J. and Kiely, C.J., 2013. Molybdenum oxide model catalysts and vanadium phosphates as actual catalysts for understanding heterogeneous catalytic partial oxidation reactions: A contribution by Jean-Claude Volta. *Catalysis Today*, 217, pp.57–64.

Wang, F., Dubois, J.-L. and Ueda, W., 2010. Catalytic performance of vanadium pyrophosphate oxides (VPO) in the oxidative dehydration of glycerol. *Applied Catalysis A: General*, 376(1), pp.25–32. Available at: http://dx.doi.org/10.1016/j.apcata.2009.11.031.

Wellauer, T.P., 1985. *Optimal Policies in Maleic Anhydride Production Through Detailed Reactor Modelling*, Swiss Federal Institute of Technology.

Wong, Y.C. and Taufiq-Yap, Y.H., 2011. Vanadyl Phosphate Dihydrate and The Vanadium Phosphate Catalyst Produced by Sonochemical Synthesis. *Asian Journal of Chemistry*, 23(9), pp.3853–3858.

Yang, W.-C., 2003. *Handbook of Fluidization and Fluid-Particle Systems* Yang, W.-C., (ed.), Marcel Dekker, Inc., United States.

Zhao, H. et al., 2016. Effects of Support for Vanadium Phosphorus Oxide Catalysts on Vapor-Phase Aldol Condensation of Methyl Acetate with Formaldehyde. *Industrial & Engineering Chemistry Research*, 55(50), pp.12693–12702. Available at: http://pubs.acs.org/doi/abs/10.1021/acs.iecr.6b03079.

APPENDICES

APPENDIX A: Reactant and Dopants Calculations

Calculations for Amount of Distilled Water Required

Mass of V_2O_5 = 60 g

Volume of o-H_3PO_4 = 360 mL

Distilled Water Required = 24 mL / g solid (Leong et al., 2011)

Distilled Water Required $= 24\ \text{mL/g solid} \times 60\ \text{g solid}$

= 1440 mL

Calculations for Amount of Dopant Required

Atomic Mass of (Haynes, 2013):

Phosphate, P	= 30.97376 g/mol	Copper, Cu	= 62.92960 g/mol
Vanadium, V	= 50.94396 g/mol	Cobalt, Co	= 58.93320 g/mol
Oxygen, O	= 15.99491 g/mol	Nitrogen, N	= 14.00307 g/mol
Hydrogen, H	= 1.00783 g/mol	Carbon, C	= 12.00000 g/mol

Molecular Weight of $VOHPO_4 \cdot 1.5H_2O$

$$= 50.94396 + 5(15.99491) + 1.00783 + 30.97376 + 1.5[2(1.00783) + 15.99491]$$

$$= 189.91596\ \text{g/mol}$$

Molecular Weight of Copper(II) nitrate, $Cu(NO_3)_2$

$$= 62.92960 + 2(14.00307 + 3(15.99491))$$

$$= 186.0952\ \text{g/mol}$$

Molecular Weight of Cobalt(II) nitrate, $Co(NO_3)_2$

$$= 58.93320 + 2(14.00307 + 3(15.99491))$$

$$= 182.9088\ \text{g/mol}$$

Mole for 15 g of $VOHPO_4 \cdot 1.5H_2O$

$$= \frac{15\ \text{g}}{189.91596\ \text{g/mol}}$$

$$= 0.07898\ \text{mol}$$

Amount of Dopant required for:

$$\text{Copper(II)nitrate 1\%} = 0.01 \times 0.07898\ \text{mol}$$

$$= 0.0007898\ \text{mol}$$

$$\text{Mass of Copper(II)nitrate} = 0.0007898\ \text{mol} \times 186.0952\ \text{g/mol}$$

$$= 0.14698\ \text{g}$$

$$\text{Cobalt(II)nitrate 1\%} = 0.01 \times 0.07898\ \text{mol}$$

$$= 0.0007898\ \text{mol}$$

$$\text{Mass of Cobalt(II)nitrate} = 0.0007898\ \text{mol} \times 182.9088\ \text{g/mol}$$

$$= 0.14446\ \text{g}$$

Catalyst	Amount of copper(II) nitrate needed (g)	Amount of cobalt(II) nitrate needed (g)
VPSBulk	-	-
VPSCu1%	0.14698	-
VPSCo1%	-	0.14446
VPSCu1%Co1%	0.14698	0.14446

APPENDIX B: Preparation of Solutions Used in Redox Titration

Preparation of 2 M H_2SO_4 Solution

Density of H_2SO_4 = 1.84 g/cm^3

Molecular weight of H_2SO_4 = 98.07 g/mol

Concentration of 95 % - 98 % H_2SO_4

$$= \frac{1.84\ \text{g/cm}^3}{98.07\ \text{g/mol}} \times \frac{95}{100} \times 1000$$

$$= 17.82\ \text{M}$$

$$M_1V_1 = M_2V_2$$

where:

M_1 = Concentration of 95 % - 98% H_2SO_4

V_2 = Volume of 95 % - 98 % H_2SO_4

M_2 = Concentration of 2 M H_2SO_4

V_1 = Volume of 2 M H_2SO_4

$$(17.82\ \text{M})(V_1) = (2\ \text{M})(1000\ \text{cm}^3)$$

$$V_1 = 112.23\ \text{cm}^3$$

Volume of 95 % - 98% H_2SO_4 required to produce 2M H_2SO_4 is 112.23 cm^3. The remaining is topped up with deionised water.

Preparation of 0.1 M H_2SO_4 Solution

$$M_1V_1 = M_2V_2$$

where:

M_1 = Concentration of 95 % - 98% H_2SO_4

V_2 = Volume of 95 % - 98 % H_2SO_4

M_2 = Concentration of 2 M H_2SO_4

V_1 = Volume of 2 M H_2SO_4

$$(17.82\ \text{M})(V_1) = (0.1\ \text{M})(1000\ \text{cm}^3)$$
$$V_1 = 5.61\ \text{cm}^3$$

Volume of 95 % - 98% H_2SO_4 required to produce 0.1 M H_2SO_4 is 5.61 cm^3. The remaining is topped up with deionised water.

Preparation of 0.01 N $KMnO_4$ Solution

$$\text{Molarity, M (mol/L)} = \frac{\text{N (eq/L)}}{\text{n (eq/mol)}}$$

$$MnO^{4-} + 8H^+ + 5e^- \longleftrightarrow Mn^{2+} + 4H_2O$$

Molarity, M

$$= \frac{0.01}{5}$$

$$= 0.002\ \text{M}$$

Molecular Weight of $KMnO_4$ is 158.04 g/mol

Weight of $KMnO_4$ in 1000 cm^3 of 0.1 M H_2SO_4

$$= 0.002\ \text{M} \times 158.04\ \text{g/mol}$$

$$= 0.3161\ \text{g}$$

0.3161 g of $KMnO_4$ crystals is dissolved in 0.1 H_2SO_4 in a 1000 mL volumetric flask.

Preparation of 0.01 N $(NH_4)_2Fe(SO_4)_2 \cdot 6H_2O$ Solution

$$\text{Molarity, M (mol/L)} = \frac{\text{N (eq/L)}}{\text{n (eq/mol)}}$$

$$Fe^{2+} + e^- \longleftrightarrow Fe^{3+}$$

Molarity, M

$$= \frac{0.01}{1}$$

$$= 0.01\ \text{M}$$

Molecular Weight of $KMnO_4$ is 391.99 g/mol

Weight of $KMnO_4$ in 1000 cm^3 of 0.1 M H_2SO_4

$= 0.01\ \text{M} \times 391.99\ \text{g/mol}$

$= 3.9199\ \text{g}$

3.9199 g of $(NH_4)_2Fe(SO_4)_2 \cdot 6H_2O$ is dissolved in 0.1 H_2SO_4 in a 1000 mL volumetric flask.

Preparation of Diphenylamine, Ph_2NH indicator

1 g of diphenylamine was weighed and dissolved in a 10 mL of concentrated H_2SO_4. Then the solution was transferred to a 100 mL volumetric flask and further top up with concentrated H_2SO_4.

APPENDIX C: Redox Titration Procedure

Solutions Preparation

1) **Preparation of Diphenylamine, Ph_2NH indicator**

   1 g of diphenylamine was weighed and dissolved in a 10 mL of concentrated H_2SO_4. Then the solution was transferred to a 100 mL volumetric flask and further top up with concentrated H_2SO_4.

2) **Preparation of 2 M H_2SO_4 Solution**

   Half of 1000 mL volumetric flask is filled with deionised water before adding 113 mL of concentrated H_2SO_4 into the volumetric flask. The remaining volume is topped up with deionised water until the meniscus of liquid reached the 1000 mL calibration mark. The volumetric flask is shaken thoroughly and allowed to be cooled.

3) **Preparation of 0.1 M H_2SO_4 Solution**

   Half of 1000 mL volumetric flask is filled with deionised water before adding 5.6 mL of concentrated H_2SO_4 into the volumetric flask. The remaining volume is topped up with deionised water until the meniscus of liquid reached the 1000 mL calibration mark. The volumetric flask is shaken thoroughly and allowed to be cooled.

4) **Preparation of 0.01 N $(NH_4)_2Fe(SO_4)_2 \cdot 6H_2O$ Solution**

   3.92 g of $(NH_4)_2Fe(SO_4)_2 \cdot 6H_2O$ is weighed and dissolved in 10 mL of concentrated H_2SO_4. Half of 1000 mL volumetric flask is filled with 0.1 M H_2SO_4 before adding the dissolved $(NH_4)_2Fe(SO_4)_2 \cdot 6H_2O$ into the volumetric flask. The remaining volume is topped up with 0.1 M H_2SO_4 until the meniscus of liquid reached the 1000 mL calibration mark. The volumetric flask is shaken thoroughly and allowed to be cooled.

5) **Preparation of 0.01 N $KMnO_4$ Solution**

   0.3161 g of $KMnO_4$ crystals is weighed and dissolved in 10 mL of concentrated H_2SO_4. Half of 1000 mL volumetric flask is filled with 0.1 M H_2SO_4 before adding the dissolved $KMnO_4$ crystals into the volumetric flask. The remaining

volume is topped up with 0.1 M H_2SO_4 until the meniscus of liquid reached the 1000 mL calibration mark. The volumetric flask is shaken thoroughly and allowed to be cooled.

6) **Preparation of Sample Solutions**

0.10 g of sample is weighed and dissolved in dissolved in 10 mL of concentrated H_2SO_4. Half of 100 mL volumetric flask is filled with 2 M H_2SO_4 before adding the dissolved sample solution into the volumetric flask. The remaining volume is topped up with 2 M H_2SO_4 until the meniscus of liquid reached the 100 mL calibration mark. The volumetric flask is shaken thoroughly and allowed to be cooled.

Experiment Set-up and Running Procedure

1) **Set-up of Apparatus**
   - Two burettes are set up using retort stand
   - One burette is filled with 0.01 N $KMnO_4$ solution
   - The other burette is filled with 0.01 N $(NH_4)_2Fe(SO_4)_2 \cdot 6H_2O$ solution
   - 100 mL sample solution is transferred to four 50 mL conical flask, each 20 mL.

2) Redox Titration Analysis
   - Two conical flask filled with sample solution is titrated with $KMnO_4$ solution and the volume is recorded as V_1. Colour changes original solution colour to pale purple.
   - Add two drop of Ph_2NH_2 indicator into all four conical flasks and gently shake it. The colour changes from purple to dark purple.
   - Two conical flasks that was titrated with $KMnO_4$ is titrated with $(NH_4)_2Fe(SO_4)_2 \cdot 6H_2O$ solution and the volume is recorded as V_2. The dark purple colour changes back to colour of original solution.
   - The remaining two conical flasks is titrated with $(NH_4)_2Fe(SO_4)_2 \cdot 6H_2O$ solution and the volume is recorded as V_3. Colour changes from dark purple to colour of original solution.

APPENDIX D: Preparation of Solutions Used for ICP-OES

Preparation of 8 M HNO_3 Solution

Density of HNO_3 = 1.4090 g/cm^3

Molecular weight of HNO_3 = 63.0130 g/mol

Concentration of 65 % HNO_3

$$= \frac{1.4090\ \text{g/cm}^3}{63.0130\ \text{g/mol}} \times \frac{65}{100} \times 1000$$

$$= 14.53\ \text{M}$$

$$M_1V_1 = M_2V_2$$

where:

M_1 = Concentration of 65 % HNO_3

V_2 = Volume of 65 % HNO_3

M_2 = Concentration of 8 M HNO_3

V_1 = Volume of 8 M HNO_3

$$(14.53\ \text{M})(V_1) = (8\ \text{M})(1000\ \text{cm}^3)$$

$$V_1 = 550\ \text{cm}^3$$

Volume of 65 % HNO_3 required to produce 8 M HNO_3 is 550 cm^3. The remaining is topped up with deionised water.

Preparation of Stock Solution for Phosphorus (P)

Molecular weight of $NH_4H_2PO_4$

$= 14.0031 + 6(1.0078) + 30.9738 + 4(15.9949)$

$= 115.0033\ \text{g/mol}$

For concentration of 50 ppm of stock solution for P,

$50\ \text{ppm} = 50\text{mg/L} = 0.05\ \text{g/L}$

Number of mole required to produce 50 ppm,

$$= \frac{0.05\ \text{g/L}}{30.9738\ \text{g/mol}}$$

$= 0.001614\ \text{mol/L}$

Mass of $NH_4H_2PO_4$ required to produce 50 ppm

$= 0.001614\ \text{mol/L} \times 115.0033\ \text{g/mol}$

$= 0.1856\ \text{g/L}$

Therefore, 0.1856 g of $NH_4H_2PO_4$ is dissolved with deionised water in a 1000 mL volumetric flask.

<u>Preparation of standard solution of phosphorus (P)</u>

$M_1V_1 = M_2V_2$

where:

M_1 = Concentration of P stock solution (50 ppm)

V_2 = Volume of P stock solution

M_2 = Concentration of standard solution

V_1 = Volume of standard solution

<u>Example calculations for standard solution of 45 ppm</u>

$(50\ \text{ppm})(V_1) = (45\ \text{ppm})(100\ \text{cm}^3)$

$V_1 = 50\ \text{cm}^3$

Volume of 50 ppm stock solution of P required to produce 45 ppm standard solution is 90 cm^3. The remaining is topped up with deionised water.

Preparation of Stock Solution for Vanadium (V)

Molecular weight of NH_4VO_3

$= 14.0031 + 4(1.0078) + 50.9440 + 3(15.9949)$

$= 116.963\ \text{g/mol}$

For concentration of 50 ppm of stock solution for V,

$50\ \text{ppm} = 50\text{mg/L} = 0.05\ \text{g/L}$

Number of mole required to produce 50 ppm,

$$= \frac{0.05\ \text{g/L}}{50.9440\ \text{g/mol}}$$

$= 0.0009815\ \text{mol/L}$

Mass of NH_4VO_3 required to produce 50 ppm

$= 0.0009815\ \text{mol/L} \times 116.963\ \text{g/mol}$

$= 0.1148\ \text{g/L}$

Therefore, 0.1148 g of NH_4VO_3 is dissolved with deionised water in a 1000 mL volumetric flask.

<u>Preparation of standard solution of vanadium (V)</u>

$M_1V_1 = M_2V_2$

where:

M_1 = Concentration of V stock solution (50 ppm)

V_2 = Volume of V stock solution

M_2 = Concentration of standard solution

V_1 = Volume of standard solution

<u>Example calculations for standard solution of 30 ppm</u>

$(50\ \text{ppm})(V_1) = (30\ \text{ppm})(100\ \text{cm}^3)$

$V_1 = 60\ \text{cm}^3$

Volume of 50 ppm stock solution of V required to produce 30 ppm standard solution is 60 cm^3. The remaining is topped up with deionised water.

Preparation of Stock Solution for Cobalt (Co)

Molecular weight of $Co(NO_3)_2$

$= 58.9332 + 2[14.0031 + 3(15.9949)]$

$= 183.9430\ \text{g/mol}$

For concentration of 50 ppm of stock solution for Co,

$50\ \text{ppm} = 50\text{mg/L} = 0.05\ \text{g/L}$

Number of mole required to produce 50 ppm,

$$= \frac{0.05\ \text{g/L}}{58.9332\ \text{g/mol}}$$

$= 0.0008484\ \text{mol/L}$

Mass of $Co(NO_3)_2$ required to produce 50 ppm

$= 0.0008484\ \text{mol/L} \times 183.9430\ \text{g/mol}$

$= 0.1561\ \text{g/L}$

Therefore, 0.1561 g of $Co(NO_3)_2$ is dissolved with deionised water in a 1000 mL volumetric flask.

<u>Preparation of standard solution of vanadium (Co)</u>

$M_1V_1 = M_2V_2$

where:

M_1 = Concentration of Co stock solution (50 ppm)

V_2 = Volume of Co stock solution

M_2 = Concentration of standard solution

V_1 = Volume of standard solution

<u>Example calculations for standard solution of 15 ppm</u>

$(50\ \text{ppm})(V_1) = (15\ \text{ppm})(100\ \text{cm}^3)$

$V_1 = 50\ \text{cm}^3$

Volume of 50 ppm stock solution of Co required to produce 15 ppm standard solution is 30 cm^3. The remaining is topped up with deionised water.

Preparation of Stock Solution for Copper (Cu)

Molecular weight of $Cu(NO_3)_2$

$= 62.9296 + 2[14.0031 + 3(15.9949)]$

$= 186.9052\ \text{g/mol}$

For concentration of 50 ppm of stock solution for Cu,

$50\ \text{ppm} = 50\text{mg/L} = 0.05\ \text{g/L}$

Number of mole required to produce 50 ppm,

$$= \frac{0.05\ \text{g/L}}{62.9296\ \text{g/mol}}$$

$= 0.0007945\ \text{mol/L}$

Mass of $Cu(NO_3)_2$ required to produce 50 ppm

$= 0.0007945\ \text{mol/L} \times 186.9052\ \text{g/mol}$

$= 0.1485\ \text{g/L}$

Therefore, 0.1485 g of $Cu(NO_3)_2$ is dissolved with deionised water in a 1000 mL volumetric flask.

<u>Preparation of standard solution of vanadium (Cu)</u>

$M_1V_1 = M_2V_2$

where:

M_1 = Concentration of Cu stock solution (50 ppm)

V_2 = Volume of Cu stock solution

M_2 = Concentration of standard solution

V_1 = Volume of standard solution

<u>Example calculations for standard solution of 5 ppm</u>

$(50\ \text{ppm})(V_1) = (5\ \text{ppm})(100\ \text{cm}^3)$

$V_1 = 50\ \text{cm}^3$

Volume of 50 ppm stock solution of Cu required to produce 5 ppm standard solution is 10 cm^3. The remaining is topped up with deionised water.

Preparation of 100 ppm sample solution

0.01 g sample in 100 mL of HNO_3

$$= \frac{0.01 \text{ g}}{100 \text{ mL } 8 \text{ M } HNO_3}$$

$$= \frac{0.01 \text{ mg}}{0.1 \text{ L } 8 \text{ M } HNO_3}$$

$$= 100 \text{ mg/L}$$

$$= 100 \text{ ppm}$$

Therefore, to produce 100 ppm of sample solution, 0.01 g of sample is dissolved in 100 cm^3 of 8 M HNO_3.

APPENDIX E: Procedure for ICP-OES Analysis

Preparation of 8 M HNO_3 Solution

About half of a 1000 cm^3 volumetric flask is filled with deionised water and 550 cm^3 of 65 % HNO_3 is measured and added into the volumetric flask. The volumetric flask is topped up with deionised water until the meniscus reached the calibration mark.

Preparation of blank HNO_3 Solution

10 cm^3 of 65 % HNO_3 is measured and added into a 100 cm^3 volumetric flask. Then, the volumetric flask is topped up with deionised water until the meniscus reached the calibration mark.

Preparation of P Standard Solution

0.1856 g of $NH_4H_2PO_4$ is weighed and added into a 50 cm^3 beaker. 10 cm^3 of HNO_3 and some deionised is added to dissolve the solid crystals. Half of 1000 cm^3 volumetric flask is filled with deionised water before transferring the dissolved sample into the volumetric flask. The volumetric flask is topped up with deionised water until the meniscus reached the calibration mark.

Five 100 cm^3 volumetric flask is prepared. For first dilution, 90 cm^3 of P stock solution is transferred to the 100 cm^3 volumetric flask and the topped up with deionised water until the calibration mark to produce 45 ppm P standard solution. For second dilution, 60 cm^3 of stock solution is transferred to the 100 cm^3 volumetric flask and the topped up with deionised water until the calibration mark to produce 30 ppm P standard solution. For third dilution, 30 cm^3 of P stock solution is transferred to the 100 cm^3 volumetric flask and the topped up with deionised water until the calibration mark to produce 15 ppm P standard solution. For fourth dilution, 20 cm^3 of P stock solution is transferred to the 100 cm^3 volumetric flask and the topped up with deionised water until the calibration mark to produce 10 ppm P standard solution. For fifth dilution, 10 cm^3 of P stock solution is transferred to the 100 cm^3 volumetric flask and the topped up with deionised water until the calibration mark to produce 5 ppm P standard solution.

Preparation of V Standard Solution

0.1148 g of NH_4VO_3 is weighed and added into a 50 cm^3 beaker. 10 cm^3 of HNO_3 and some deionised is added to dissolve the solid crystals. Half of 1000 cm^3 volumetric flask is filled with deionised water before transferring the dissolved sample into the volumetric flask. The volumetric flask is topped up with deionised water until the meniscus reached the calibration mark.

Five 100 cm^3 volumetric flask is prepared. For first dilution, 90 cm^3 of V stock solution is transferred to the 100 cm^3 volumetric flask and the topped up with deionised water until the calibration mark to produce 45 ppm V standard solution. For second dilution, 60 cm^3 of V stock solution is transferred to the 100 cm^3 volumetric flask and the topped up with deionised water until the calibration mark to produce 30 ppm V standard solution. For third dilution, 30 cm^3 of V stock solution is transferred to the 100 cm^3 volumetric flask and the topped up with deionised water until the calibration mark to produce 15 ppm V standard solution. For fourth dilution, 20 cm^3 of V stock solution is transferred to the 100 cm^3 volumetric flask and the topped up with deionised water until the calibration mark to produce 10 ppm V standard solution. For fifth dilution, 10 cm^3 of V stock solution is transferred to the 100 cm^3 volumetric flask and the topped up with deionised water until the calibration mark to produce 5 ppm V standard solution.

Preparation of Co Standard Solution

0.1561 g of $Co(NO_3)_2$ is weighed and added into a 50 cm^3 beaker. 10 cm^3 of HNO_3 and some deionised is added to dissolve the solid crystals. Half of 1000 cm^3 volumetric flask is filled with deionised water before transferring the dissolved sample into the volumetric flask. The volumetric flask is topped up with deionised water until the meniscus reached the calibration mark.

Five 100 cm^3 volumetric flask is prepared. For first dilution, 90 cm^3 of Co stock solution is transferred to the 100 cm^3 volumetric flask and the topped up with deionised water until the calibration mark to produce 45 ppm Co standard solution. For second dilution, 60 cm^3 of Co stock solution is transferred to the 100 cm^3 volumetric flask and the topped up with deionised water until the calibration mark to produce 30 ppm Co standard solution. For third dilution, 30 cm^3 of Co stock solution is transferred to the 100 cm^3 volumetric flask and the topped up with deionised water until the calibration mark to produce 15 ppm Co standard solution. For fourth dilution, 20 cm^3 of Co stock

solution is transferred to the 100 cm^3 volumetric flask and the topped up with deionised water until the calibration mark to produce 10 ppm Co standard solution. For fifth dilution, 10 cm^3 of Co stock solution is transferred to the 100 cm^3 volumetric flask and the topped up with deionised water until the calibration mark to produce 5 ppm Co standard solution.

Preparation of Cu Standard Solution

0.1485 g of $Cu(NO_3)_2$ is weighed and added into a 50 cm^3 beaker. 10 cm^3 of HNO_3 and some deionised is added to dissolve the solid crystals. Half of 1000 cm^3 volumetric flask is filled with deionised water before transferring the dissolved sample into the volumetric flask. The volumetric flask is topped up with deionised water until the meniscus reached the calibration mark.

Five 100 cm^3 volumetric flask is prepared. For first dilution, 90 cm^3 of Cu stock solution is transferred to the 100 cm^3 volumetric flask and the topped up with deionised water until the calibration mark to produce 45 ppm Cu standard solution. For second dilution, 60 cm^3 of Cu stock solution is transferred to the 100 cm^3 volumetric flask and the topped up with deionised water until the calibration mark to produce 30 ppm Cu standard solution. For third dilution, 30 cm^3 of Cu stock solution is transferred to the 100 cm^3 volumetric flask and the topped up with deionised water until the calibration mark to produce 15 ppm Cu standard solution. For fourth dilution, 20 cm^3 of Cu stock solution is transferred to the 100 cm^3 volumetric flask and the topped up with deionised water until the calibration mark to produce 10 ppm Cu standard solution. For fifth dilution, 10 cm^3 of Cu stock solution is transferred to the 100 cm^3 volumetric flask and the topped up with deionised water until the calibration mark to produce 5 ppm Cu standard solution.

Preparation of Sample Solution

To produce 100 ppm of sample solution, 0.01 g of sample is dissolved in 100 cm^3 of 8 M HNO_3.

APPENDIX F: P/V Atomic Ratio from ICP-OES analysis

Calculations of P/V atomic ratio using data obtained from ICP-OES analysis

$$\frac{\mathrm{P}}{\mathrm{V}} = \frac{\text{Concentration of P / Atomic Weight of P}}{\text{Concentration of V / Atomic Weight of V}}$$

Example calculations

For VPOBulk:

Average concentration of P = 3.380 mg/L

Average concentration of V = 5.121 mg/L

Atomic Mass of Phosphate, P = 30.9738 g/mol

Atomic Mass of Vanadium, V = 50.9440 g/mol

$$\frac{\mathrm{P}}{\mathrm{V}} = \frac{3.380\ \text{mg/L} \div 30.9738\ \text{g/mol}}{5.121\ \text{mg/L} \div 50.9440\ \text{g/mol}}$$

$$= 1.0855$$

APPENDIX G: Calculation for Average Oxidation State of Vanadium (V_{AV})

Calculations of P/V atomic ratio using data obtained from ICP-OES analysis

According to Niwa and Murakami,

$V^{4+} + 2V^{3+}$ = 20 $[MnO_4^-]$ V_1

$V^{5+} + V^{4+} + V^{3+}$ = 20 $[Fe^{2+}]$ V_2

V^{5+} = 20 $[Fe^{2+}]$ V_3

$[MnO_4^-]$ = 0.01 N

$[Fe^{2+}]$ = 0.01 N

$V^{4+} + 2V^{3+}$ = 0.2 V_1 (1)

$V^{5+} + V^{4+} + V^{3+}$ = 0.2 V_2 (2)

V^{5+} = 0.2 V_3 (3)

Equation (2) – (3),

$V^{4+} + V^{3+}$ = 0.2 V_2 – 0.2 V_3

V^{4+} = 0.2 V_2 – 0.2 V_3 – V^{3+} (4)

Substitute Equation (4) in (1) and rearrange,

V^{3+} = 0.2 V_1 – 0.2 V_2 + 0.2 V_3 (5)

Substitute Equation (5) in (4)

V^{4+} = 0.4 V_2 – 0.4 V_3 - 0.2 V_1

Thus,

V^{3+} = 0.2 V_1 – 0.2 V_2 + 0.2 V_3

V^{4+} = 0.4 V_2 – 0.4 V_3 - 0.2 V_1

V^{5+} = 0.2 V_3

Average Oxidation State:

$$V_{AV} = \frac{3V^{3+} + 4V^{4+} + 5V^{5+}}{V^{3+} + V^{4+} + V^{5+}}$$

Example calculations

For VPOBulk:

Average V_1 = 5.45

Average V_2 = 6.85

Average V_3 = 7.9

V^{3+} = 0.2 (5.45) – 0.2 (6.85) + 0.2 (7.9) = 1.3

V^{4+} = 0.4 (6.85) – 0.4 (7.9) - 0.2 (5.45) = 1.51

V^{5+} = 0.2 (7.9) = 1.58

$$V_{AV} = \frac{3(1.3) + 4(1.51) + 5(1.58)}{1.3 + 1.51 + 1.58}$$

$$= 4.2044$$

The calculated results are tabulated as table below:

VPOBulk	**$KMnO_4$ V_1**		**$(NH_4)_2Fe(SO_4)_2$ V_2**		**$(NH_4)_2Fe(SO_4)_2$ V_3**	
	1	2	1	2	1	2
Initial (cm^3)	0	5.3	0	6.9	0	7.9
Final (cm^3)	5.3	10.9	6.9	13.6	7.9	15.8
Volume used (cm^3)	5.3	5.6	6.9	6.8	7.9	7.9
Average	5.45		6.85		7.9	
V_{AV} = 4.2044	V^{4+} = 79.56 %				V^{5+} = 20.44 %	

VPOCo1%	**$KMnO_4$ V_1**		**$(NH_4)_2Fe(SO_4)_2$ V_2**		**$(NH_4)_2Fe(SO_4)_2$ V_3**	
	1	2	1	2	1	2
Initial (cm^3)	0	5.9	0	7.0	0	6.5
Final (cm^3)	5.9	11.8	7.0	14.4	6.5	12.9
Volume used (cm^3)	5.9	5.9	7.0	7.4	6.5	6.4
Average	5.9		7.2		6.45	
V_{AV} = 4.1806	V^{4+} = 81.94 %				V^{5+} = 18.06 %	

VPOCu1%	**$KMnO_4$ V_1**		**$(NH_4)_2Fe(SO_4)_2$ V_2**		**$(NH_4)_2Fe(SO_4)_2$ V_3**	
	1	2	1	2	1	2
Initial (cm^3)	0	6.2	0	8.3	16.3	23.5
Final (cm^3)	6.2	12.3	8.3	16.3	23.5	30.9
Volume used (cm^3)	6.1	6.1	8.3	8.0	7.2	7.4
Average	6.15		8.15		7.3	
$\mathbf{V_{AV}}$ = 4.2454	V^{4+} = 75.46 %				V^{5+} = 24.54 %	

VPOCu1%Co1%	**$KMnO_4$ V_1**		**$(NH_4)_2Fe(SO_4)_2$ V_2**		**$(NH_4)_2Fe(SO_4)_2$ V_3**	
	1	2	1	2	1	2
Initial (cm^3)	0	9.3	0	8.9	0	7.1
Final (cm^3)	9.3	18.4	8.9	17.5	7.1	7.2
Volume used (cm^3)	5.7	5.9	8.5	8.2	7.1	7.3
Average	5.8		8.35		7.2	
$\mathbf{V_{AV}}$ = 4.3054	V^{4+} = 69.46 %				V^{5+} = 30.54 %	

APPENDIX H: Calculation for Reduction Activation Energy (E_r) for TPR Analysis

Required Formulas to Calculate Reduction Activation Energy (E_r)

$$E_a = T_m \times 0.066$$

where T_m = temperature maxima

where A = 1×10^{13}

$$\chi = Ae^{\left(\frac{-E_a}{RT_m}\right)}$$

R = 0.001987 kcal K^{-1} mol^{-1}

χ = 0.03754 s^{-1}

where P = Pressure (atm)

$$[H_2] = \frac{P}{RT}$$

T = Ambient temperature (298 K)

R = 82.056 cm^3 atm K^{-1} mol

$[H_2]$ = 4.036×10^{-7} mol cm^3

$$E_r = RT_m \ln\left[\frac{A(H_2)}{\chi}\right]$$

where R = 0.001987 kcal K^{-1} mol^{-1}

Example Calculations

For VPOBulk,

Peak 1 (T_m = 703 K):

$$E_r = RT_m \ln\left[\frac{A(H_2)}{\chi}\right]$$

$$= (0.001987)(703) \ln\left[\frac{(1 \times 10^{13})(4.306 \times 10^{-7})}{0.03754}\right]$$

$$= 108.0824 \text{ kJ/mol}$$

Peak 2 (T_m = 932 K):

$$E_r = RT_m \ln\left[\frac{A(H_2)}{\chi}\right]$$

$$= (0.001987)(932) \ln\left[\frac{(1 \times 10^{13})(4.306 \times 10^{-7})}{0.03754}\right]$$

$$= 143.2899 \text{ kJ/mol}$$

APPENDIX I: Calculation for Amount of Oxygen Removed

Formulas Required to Calculate Amount of Oxygen Removed

Amount of oxygen removed

$$= \text{amount of oxygen (mol/g)} \times \text{Avogadro's number (atom/g)}$$

$$= \text{amount of oxygen (mol/g)} \times 6.02 \times 10^{23}\ \text{atom/g}$$

Example Calculations

For VPOBulk,

Peak 1:

$$\text{Amount of oxygen removed} = 76.74359\ \mu\text{mol/g}$$

$$= 7.67 \times 10^{-5}\ \text{mol/g}$$

$$= 7.67 \times 10^{-5}\ \text{mol/g} \times 6.02 \times 10^{23}\ \text{atom/g}$$

$$= 4.62 \times 10^{19}\ \text{atom/g}$$

Peak 2:

$$\text{Amount of oxygen removed} = 169.48831\ \mu\text{mol/g}$$

$$= 1.69 \times 10^{-4}\ \text{mol/g}$$

$$= 1.69 \times 10^{-4}\ \text{mol/g} \times 6.02 \times 10^{23}\ \text{atom/g}$$

$$= 1.02 \times 10^{20}\ \text{atom/g}$$